PAPC mediates self/non–self-distinction during Snail1-dependent tissue separation

Olivia Luu,[1] Erich W. Damm,[1] Serge E. Parent,[1] Debanjan Barua,[1] Tamara H.L. Smith,[1] Jason W.H. Wen,[1] Stephanie E. Lepage,[1] Martina Nagel,[1] Hady Ibrahim-Gawel,[2] Yunyun Huang,[1] Ashley E.E. Bruce,[1] and Rudolf Winklbauer[1]

[1]Department of Cell and Systems Biology, University of Toronto, Toronto, Ontario, Canada M5S 3G5
[2]Zoological Institute, University of Cologne, D-50674 Cologne, Germany

Cleft-like boundaries represent a type of cell sorting boundary characterized by the presence of a physical gap between tissues. We studied the cleft-like ectoderm–mesoderm boundary in *Xenopus laevis* and zebrafish gastrulae. We identified the transcription factor Snail1 as being essential for tissue separation, showed that its expression in the mesoderm depends on noncanonical Wnt signaling, and demonstrated that it enables paraxial protocadherin (PAPC) to promote tissue separation through two novel functions. First, PAPC attenuates planar cell polarity signaling at the ectoderm–mesoderm boundary to lower cell adhesion and facilitate cleft formation. Second, PAPC controls formation of a distinct type of adhesive contact between mesoderm and ectoderm cells that shows properties of a cleft-like boundary at the single-cell level. It consists of short stretches of adherens junction–like contacts inserted between intermediate-sized contacts and large intercellular gaps. These roles of PAPC constitute a self/non–self-recognition mechanism that determines the site of boundary formation at the interface between PAPC-expressing and -nonexpressing cells.

Introduction

Cell-impermeable boundaries are essential for the maintenance of tissue integrity. One distinct type of boundary is characterized by a narrow cleft between tissues, such as that which separates newly formed somites or hindbrain rhombomeres. Often, these clefts mature into ECM-filled spaces during development (Tepass et al., 2002). Another example of this type of boundary is Brachet's cleft, which separates the ectoderm from the mesoderm in *Xenopus laevis* gastrulae. It permits the mesodermal cell mass to migrate across the multilayered ectodermal blastocoel roof (BCR) without invading it (Winklbauer, 2009). In zebrafish gastrulae, the mesendodermal hypoblast is similarly separated from the ectodermal epiblast (Kimmel et al., 1995).

Eph/ephrin signaling is required for tissue separation at Brachet's cleft. Eph receptor tyrosine kinases generally interact with membrane-linked ephrin ligands, initiating receptor forward signaling or reverse signaling through the ligand. In *Xenopus*, numerous Ephs and ephrins are coexpressed in the ectoderm and mesoderm, and antiparallel forward signaling from the ectoderm to the mesoderm and vice versa induce cell repulsion at the boundary (Rohani et al., 2011; Park et al., 2011). The coexpression of Ephs with their ligands raises the question of why repulsion occurs only at the boundary but not also within each tissue, which would compromise tissue integrity. In part, this is caused by quantitative differences in receptor and ligand isoform expression that, in combination with the selectivity of receptor–ligand interactions, confer the highest levels of Eph/ephrin signaling to the ectoderm–mesoderm boundary (Rohani et al., 2014). Here, we show that an additional mechanism is required for boundary formation.

Paraxial protocadherin (PAPC) is a central factor in this mechanism, which acts in parallel to Eph signaling. PAPC (Kim et al., 1998; Hukriede et al., 2003; Medina et al., 2004; Schambony and Wedlich, 2007) and a PAPC effector, ankyrin repeat domain protein 5 (xANR5; Chung et al., 2007), have been shown

Correspondence to Rudolf Winklbauer: r.winklbauer@utoronto.ca; or Ashley E.E. Bruce: ashley.bruce@utoronto.ca

H. Ibrahim-Gawel's present address is QIAGEN GmbH, 40724 Hilden, Germany.

Abbreviations used in this paper: ADSA, axisymmetric drop shape analysis; BCR, blastocoel roof; CA, constitutively active; CB, cacodylate buffer; DN, dominant negative; FDA, fluorescein-dextran; GA, glutaraldehyde; LN, lanthanum nitrate; MBS, modified Barth's solution; MO, morpholino antisense oligonucleotide; PAPC, paraxial protocadherin; PCP, planar cell polarity; PTX, pertussis toxin; RDA, rhodamine-dextran; SEM, scanning EM; TEM, transmission EM.

The Rockefeller University Press $30.00
J. Cell Biol. Vol. 208 No. 6 839–856
www.jcb.org/cgi/doi/10.1083/jcb.201409026

previously to effect tissue separation in collaboration with an Xfz7-PKC noncanonical Wnt pathway (Winklbauer et al., 2001). In the present study, we show that Fz7 also signals through a Dvl-RhoA-JNK-cJun cascade to promote the expression of Snail1 (Sargent and Bennett, 1990; Hammerschmidt and Nüsslein-Volhard, 1993). Snail transcription factors affect adhesion, motility, epithelial–mesenchymal transition, and tumor progression (Thiery, 2002; Barrallo-Gimeno and Nieto, 2005; Speirs et al., 2010), and we show here that Snail1 enables PAPC to function in tissue separation. PAPC down-regulates planar cell polarity (PCP) signaling (Mlodzik, 2002) at the tissue boundary, apparently to reduce adhesion across Brachet's cleft. PAPC also controls a self/non–self-recognition process that establishes an adhesive, yet flexible, contact between ectoderm and mesoderm cells. Our findings integrate new and previously identified control modules and outline the mechanism underlying tissue separation at the prechordal mesoderm.

Results

Noncanonical Fz7 signaling controls tissue separation through Snail1 expression

Xsnail1 is expressed in the mesoderm of *Xenopus* gastrulae (Essex et al., 1993). To identify its function, morpholino antisense oligonucleotides (MOs) were injected into dorsal blastomeres. In uninjected or 5-mismatch control MO (5mis-MO)–injected embryos, Brachet's cleft separated the prechordal mesoderm from the ectodermal BCR (Fig. 1 A). Injection of Snail1-MO eliminated cleft formation in this region (Fig. 1 B), and coinjection of Xsnail1 mRNA rescued it (Fig. 1 C), suggesting that Xsnail1 is required for tissue separation. Cleft defects in Xsnail1 morphants were not accompanied by any noticeable changes in mesoderm specification (Fig. S1, A–D).

Tissue separation can be tested on explanted BCR by using a standard assay (Fig. 1, D–G; Winklbauer and Keller, 1996; Wacker et al., 2000; Winklbauer et al., 2001). Normally, prechordal mesoderm explants remain on the BCR surface, showing separation behavior, whereas ectodermal BCR explants sink into the BCR. In accordance with the gastrula phenotype, control 5mis-MO had no effect on separation behavior (Fig. 1, D and H), whereas Xsnail1-MO–injected mesoderm integrated into the BCR (Fig. 1, E and H). Furthermore, separation behavior was rescued by coinjection of Xsnail1 mRNA (Fig. 1, F and H). These results indicate that Xsnail1 is necessary for ectodermal–mesodermal tissue separation.

Snail1 is also essential for tissue separation in zebrafish gastrulae. Brachet's cleft, which forms between the ectodermal epiblast and mesendodermal hypoblast was disrupted by injection of Snail1a-MO, but not by a 5mis-MO (Fig. 1 J). Moreover, when pieces of mesoderm or epiblast were placed on epiblast explants in a manner analogous to the *Xenopus* BCR assay, epiblast aggregates sunk in reliably, whereas mesoderm aggregates remained on the surface (Fig. 1, I and K). Snail1a-MO caused the mesoderm to sink into the epiblast, whereas 5mis-MO had no such effect (Fig. 1 I and Fig. S1, E and F). Coinjection of Snail1a mRNA with Snail1a-MO rescued separation behavior (Fig. 1 I and Fig. S1 G).

We next asked how Xfz7 signaling (Winklbauer et al., 2001) relates to Xsnail1 function during tissue separation. We confirmed that Xfz7b-MO diminishes separation behavior (Fig. 2 A). Coinjection of Xsnail1 mRNA rescued separation (Fig. 2 A), placing Xsnail1 downstream of Xfz7. Indeed, Xsnail1 expression was regulated by Xfz7b (Fig. 2, B and C). Xsnail1 is expressed in the involuting mesoderm. Xfz7b-MO reduced its expression, and this effect was reversed by Xfz7b mRNA. Constitutively active (CA) JNK also rescued Xsnail1 expression, and the JNK inhibitor SP600125 diminished it, indicating that Xfz7b acts through JNK. A target of JNK is the transcription factor c-Jun; MOs against two closely related c-Jun genes (Knöchel et al., 2000) inhibited Xsnail1 expression except in the most posterior region. c-Jun mRNA rescued Xsnail1 expression in c-Jun–MO and in Xfz7b-MO embryos, placing c-Jun downstream of Xfz7-JNK. Xsnail1 expression appeared mislocalized after some treatments because of aberrant gastrulation movements (Fig. 2 B). The JNK inhibitor SP600125 strongly affected separation, and injection of Xsnail1 mRNA mitigated this effect (Fig. 2 A). Similarly, c-Jun–MO diminished separation, and both c-Jun and Xsnail1 mRNAs rescued it. CA-JNK and c-Jun mRNA rescued separation in Xfz7b-MO–injected mesoderm (Fig. 2 A). Together, these results indicate that Xfz7/JNK/c-Jun signaling controls Xsnail1 expression, which is in turn essential for separation behavior.

During noncanonical Wnt signaling, Fz activates JNK through Dvl and any of the GTPases RhoA, Rac, or Cdc42 (Boutros et al., 1998; Bikkavilli et al., 2008 and references therein). We characterized this link in our system. Knockdown of *Xenopus* Dvl2 strongly reduced Xsnail1 expression; coinjection of CA-JNK restored this expression, confirming that Dvl acts through JNK (Fig. 2 B). Of the dominant-negative (DN) forms of Rac, Cdc42, and RhoA, only DN-RhoA inhibited Xsnail1 expression (Fig. 2 B). Expression could be rescued by CA-JNK (Fig. 2 B), placing RhoA upstream of JNK. Because of the multiple functions of RhoA and Dvl2, their complex effects are treated separately below.

In the noncanonical Wnt pathway, which controls convergent extension of *Xenopus* chordamesoderm, the formin protein Daam1 links Dvl to RhoA activation (Habas et al., 2001; Liu et al., 2008; Tanegashima et al., 2008). However, neither N-Daam1 nor DN T-Daam1 inhibited Xsnail1 expression (Fig. 2 B and not depicted), nor did Daam1-MO or N-Daam1 diminish separation behavior (Fig. 2 A). Thus, Daam1 does not mediate the signal from Dvl2 to RhoA to regulate Xsnail1 expression.

In the zebrafish, the upstream control of Snail1a is similar to that in *Xenopus*. DN-RhoA reduced Snail1a expression, and expression could be rescued by CA-JNK (Fig. 2 D). In addition, an MO directed against the zebrafish dvl2 isoform diminished Snail1a expression (Fig. 2 D). Although knockdown of zebrafish Fz7b had no effect, expression of the cytoplasmically truncated Xfz7ΔC (Winklbauer et al., 2001) reduced Snail1a expression (Fig. 2 D). These data are consistent with Snail1a being regulated through an Fz7-Dvl2-RhoA-JNK module, although the Fz7 isoform involved has yet to be determined.

Together, these results suggest that Fz7 acts through Dvl and the activation of RhoA, JNK, and c-Jun to up-regulate

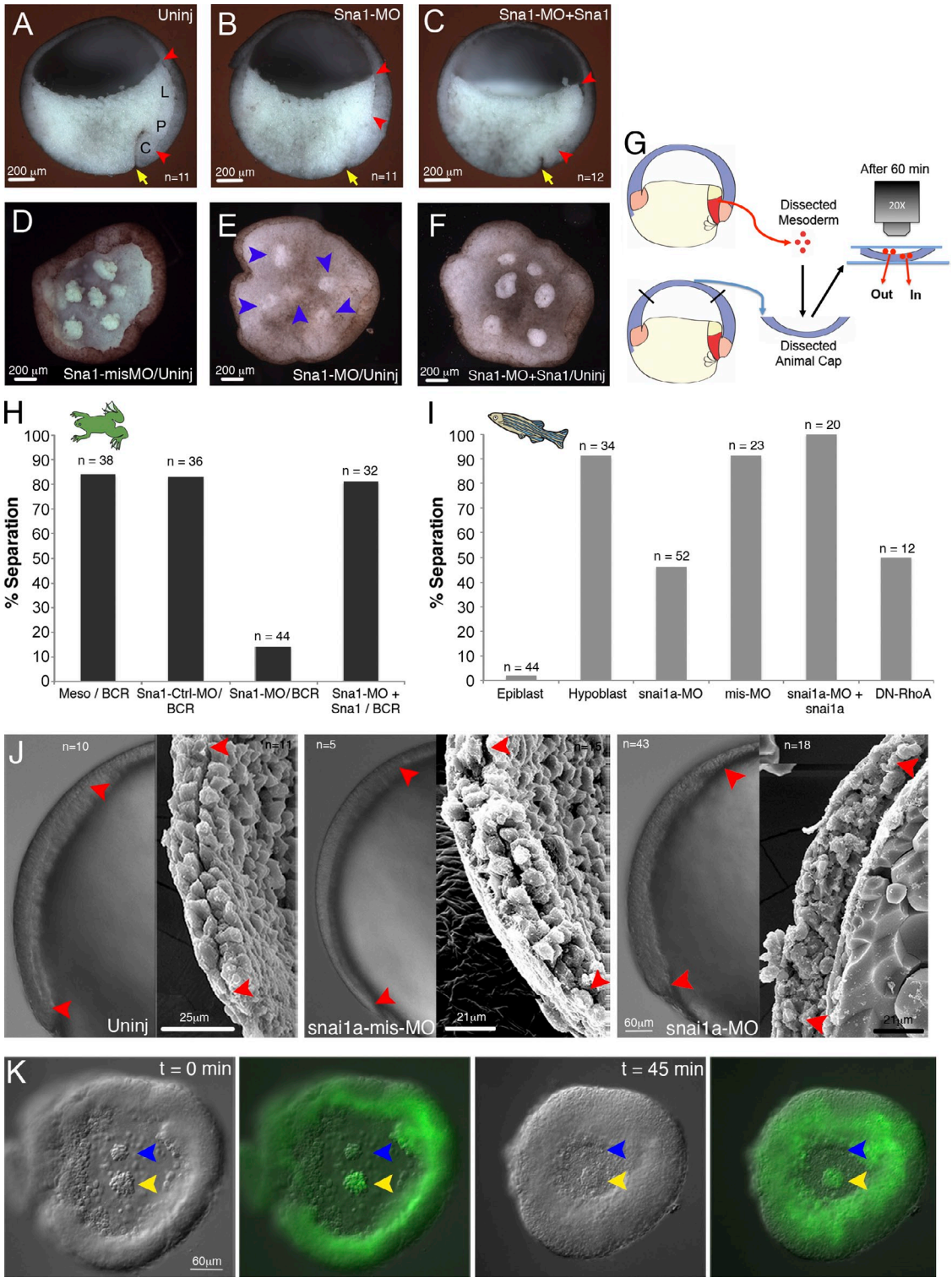

Figure 1. **Snail1 function in tissue separation.** (A–C) Brachet's cleft in sagittally fractured stage 10.5 *Xenopus* gastrulae. Uninjected embryos (A); cleft (between red arrowheads) is shortened by Xsnail1-MO (B), but not Xsnail1-MO/Xsnail1 mRNA coinjection (C). Yellow arrows indicate the blastopore. C, chordamesoderm; P, prechordal mesoderm; L, leading edge mesendoderm; n, number of embryos. (D–F) BCR assay for separation behavior in *Xenopus*. Prechordal mesoderm explants injected with control Sna1-misMO (D), Xsnail1-MO (E), or Xsnail1-MO and Xsnail1 mRNA (F) are placed on explanted BCR. Explants sunken after 1 h in E are indicated by arrowheads. (G) Outline of BCR assay. (H) Quantitation of BCR assay. Y axis, percentage of test explants remaining on surface; n, number of explants. (I–K) Tissue separation in zebrafish. (I) Quantitation of separation behavior as in H. (J) Brachet's cleft in live embryos (left panels) and SEM micrographs (right panels) at 75% epiboly in wild-type and *snai1a*-misMO– and *snail1a* MO–injected embryos. Red arrowheads indicate Brachet's cleft; n, number of embryos. (K) In vitro assay, differential interference contrast images, and fluorescence overlay images at explanation (left) and 45 min later (right). Epiblast test explant (blue arrowheads) sinks into the epiblast, and fluorescent hypoblast explant (yellow arrowheads) remains on the surface.

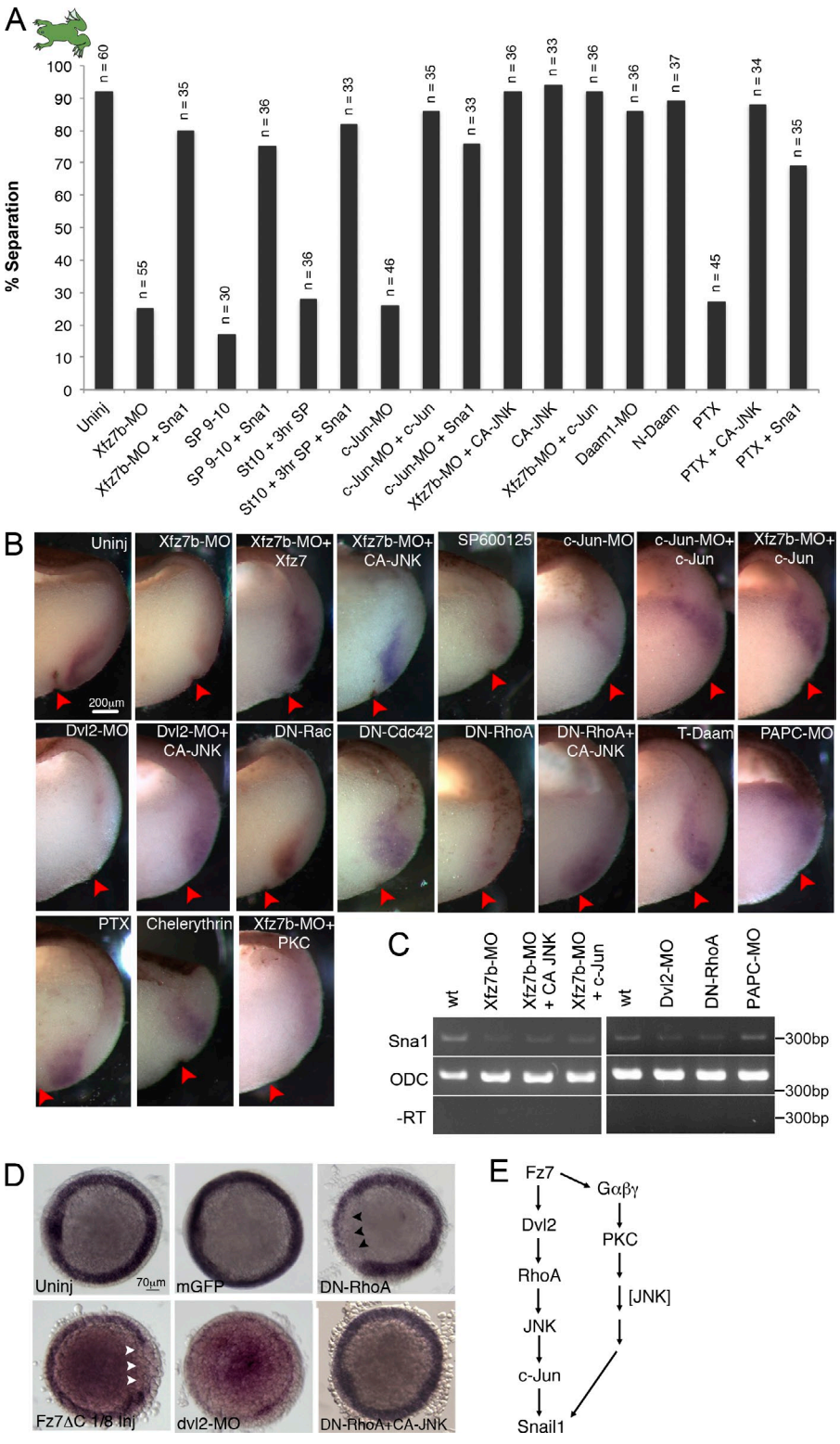

Figure 2. **Xfz7 signaling regulates Xsnail1 expression and separation behavior.** (A) Quantitative analysis of tissue separation as in Fig. 1 (H and I). Mesoderm was injected as indicated (symbols as in the text). (B) In situ hybridization for Xsnail1 RNA in stage 10.5 *Xenopus* gastrulae; dorsal halves of sagittally fractured embryos are shown. Red arrowheads indicate blastopore; differences in morphology caused by effects of treatments on gastrulation movements. (C) RT-PCR of dorsal mesoderm from stage 10.5 gastrulae to detect Xsnail1 mRNA. (D) *snail1a* in situ hybridization in zebrafish. Expression is normal in uninjected and *mgfp* RNA–injected embryos, reduced in DN-RhoA embryo (black arrowheads), and rescued in embryo coinjected with DN-RhoA and CA-JNK mRNA. Xfz7ΔC injected into one of eight blastomeres (white arrowheads) and dvl2-MO inhibit Snail1a expression. (E) Inferred pathway of Snail1 expression control by Fz7.

Snail1 expression (Fig. 2 E). This cascade is distinct from the noncanonical pathway that regulates chordamesoderm convergent extension in *Xenopus* (Wallingford et al., 2002; Kim and Han, 2005; Roszko et al., 2009), but similar to the Fz/JNK/Jun cascade that controls PCP in the *Drosophila melanogaster* eye.

We showed previously that Xfz7-Gαβγ-PKC signaling also controls tissue separation (Winklbauer et al., 2001). Inhibition of G protein function with pertussis toxin (PTX; Winklbauer et al., 2001) or treatment with the PKC inhibitor chelerythrine did not affect Xsnail1 expression, and Xfz7b-MO–reduced Xsnail1 expression could not be rescued by PKC mRNA (Fig. 2 B). Thus, Xfz7-Gαβγ-PKC signaling is necessary for separation but not for Xsnail1 expression. However, Xsnail1 and CA-JNK each rescued tissue separation upon Xfz7b-MO knockdown or

PTX inhibition (Fig. 2 A), suggesting that the Gαβγ-PKC branch acts upstream of Xsnail1 and involves JNK activation (Fig. 2 E).

Snail1 enables PAPC function in tissue separation

PAPC is proposed to act synergistically with Xfz7 during tissue separation (Medina et al., 2004). PAPC-MO indeed reduced separation behavior, but morphants could not be rescued by CA-JNK or Xsnail1 mRNA (Fig. 3 A), and PAPC-MO did not diminish Xsnail1 expression (Fig. 2, B and C). Moreover, PAPC coexpression was not essential for induction of Xsnail1 expression in the BCR by Xfz7b (Fig. 3 C). Thus, PAPC does not act on Xsnail1 expression through the Xfz7/JNK/Jun pathway. Conversely, PAPC expression was not induced by Xsnail1 mRNA in the BCR (Fig. 3 D), indicating that Xsnail1 and PAPC are regulated independently and that both factors are required for tissue separation. In the zebrafish, knockdown of the PAPC homologue pcdh8 also inhibited separation behavior, and separation could be rescued by pcdh8 mRNA (Fig. 3 B).

Cooperation of Snail1 and PAPC was shown in gain-of-function experiments (Fig. 3 E). Coexpression of Xfz7b and PAPC induced separation behavior in the ectodermal BCR (Fig. 3 E; Medina et al., 2004). This effect depended on Xsnail1, as coinjection of Xsnail1-MO strongly reduced separation (Fig. 3 E). Xsnail1 mRNA, at a dose which rescued separation behavior in the mesoderm, had no effect in the BCR. PAPC mRNA alone was also ineffective, but coinjection of Xsnail1 and PAPC mRNA induced separation behavior (Fig. 3 E). These results imply that Xfz7b and PAPC interact indirectly.

PAPC function in tissue separation is mediated by XANR5 (Chung et al., 2007). Its baseline expression in the BCR was not up-regulated by Xsnail1 (Fig. S2 A), and adding XANR5 alone or together with PAPC barely induced separation behavior in the BCR (Fig. 3 E). Thus, a normal level of XANR5 in the ectoderm is sufficient, but PAPC function requires an additional Xsnail1-dependent factor. In contrast, the membrane-tethered extracellular domain of PAPC, M-PAPC, is sufficient to cause cell sorting (Kim et al., 1998; Ninomiya and Winklbauer, 2008), rescue tissue separation upon Xsnail1 knockdown (Fig. 3 A), and induce separation ectopically in the BCR (Fig. 3 M). These data imply that XANR5 activity is equivalent to the removal of the PAPC cytoplasmic domain, e.g., by blocking an autoinhibitory function. Snail1 could control PAPC at the same level by regulating the expression of a PAPC-interacting factor. In conclusion, PAPC is essential for tissue separation and Snail1 enables full-length PAPC function (Fig. 3 F), whereas M-PAPC acts in a Snail1-independent manner.

PAPC promotes self/non-self-recognition and cleft contact formation

To further define the role of PAPC, we induced ectopic cleft formation in the BCR (Fig. 3, G–L). Expression of either Xsnail1 or PAPC in half of the BCR did not induce boundary formation (Fig. 3, G and H); however, coexpression of these factors caused tissue separation along the expression boundary (Fig. 3 I), confirming the co-requirement for these factors. The Xsnail1-independent M-PAPC construct also induced tissue separation (Fig. 3 J). Separation was not caused by altered levels of Ephs and ephrins; no differential regulation of any of these factors was observed in BCR expressing Xsnail1 and PAPC (Fig. S2, B and C). Moreover, EphB4 overexpression or ephrinB1/ephrinB2 knockdown in half of the BCR did not induce a cleft (Fig. S2, D and E). Thus, PAPC/Xsnail1 can elicit ectopic boundary formation without modulating the Eph/ephrin complement of the BCR.

When PAPC was expressed throughout the BCR and Xsnail1 was coexpressed on one side, no boundary formed (Fig. 3 K), but separation occurred in the converse experiment (Fig. 3 L). Thus, apposition of PAPC-expressing ($PAPC^+$) and -nonexpressing ($PAPC^-$) cells is required to determine the boundary, whereas Snail1 enables PAPC function. In agreement with this notion, ectopic PAPC in the BCR attenuated its separation from the mesoderm, which endogenously expresses PAPC and Snail1 (Fig. 3 M and Fig. S2 F). Although no cleft formed, expression of PAPC and Xsnail1 in adjacent halves of the BCR led to the formation of a sorting boundary that often prevented cell mixing (Fig. S3). Such an effect could be relevant when a boundary is determined by the apposition of Snail1-expressing and nonexpressing tissue, such as in the case of the notochord-somite boundary in the ascidian *Ciona* (Fujiwara et al., 1998).

Despite its homophilic binding ability (Kim et al., 2011), PAPC does not promote adhesion (Chen and Gumbiner, 2006). Moreover, M-$PAPC^+$ and M-$PAPC^-$ cells sort out when mixed, but have no strong preference for interior or surface positions, respectively (Kim et al., 1998; Ninomiya and Winklbauer, 2008), and we found that PAPC indeed does not generate an adhesion difference: tissue surface tension, a measure of cell–cell adhesion (Manning et al., 2010; David et al., 2014), was not altered by M-PAPC expression in the BCR (Fig. 3 N). This argues against a differential adhesion mechanism of boundary formation and suggests a localized modulation of adhesive interactions between M-$PAPC^+$ and M-$PAPC^-$ cells.

To examine this interaction, we reaggregated mixtures of M-$PAPC^+$ and M-$PAPC^-$ BCR cells (Fig. 4 A; Fig. S4, A and B; and Videos 1 and 2). Cells of the same type attached rapidly. M-$PAPC^+$ and M-$PAPC^-$ cells also formed stable contacts, but appeared to remain separated by a narrow gap when cells were visualized by injected fluorescent dextran (Fig. 4, A, C, and E; and Fig. S4 B). Although these heterotypic contacts resisted pulling, cells slipped easily past each other at these gap-like interfaces (Fig. 4 A and Videos 1 and 2). Thus, although tight contacts between cells of the same type appeared similar (Fig. 4, A, C, and E), contacts between different cell types appeared cleft-like, yet adhesive and permitted rapid lateral exchange of cell neighbors. Herein, we refer to these adhesive structures as cleft contacts.

Cleft contacts depended on Eph signaling. Gaps between M-$PAPC^+$ and M-$PAPC^-$ cells were stable, but EphB4 knockdown in M-$PAPC^+$ cells caused prolonged gap occlusions (Fig. 4, C and E; Fig. S4 C; and Video 3). Cleft contacts also formed between prechordal mesoderm and BCR cells, with lateral gliding occurring at rates of up to 2–3 µm/min and cells separating

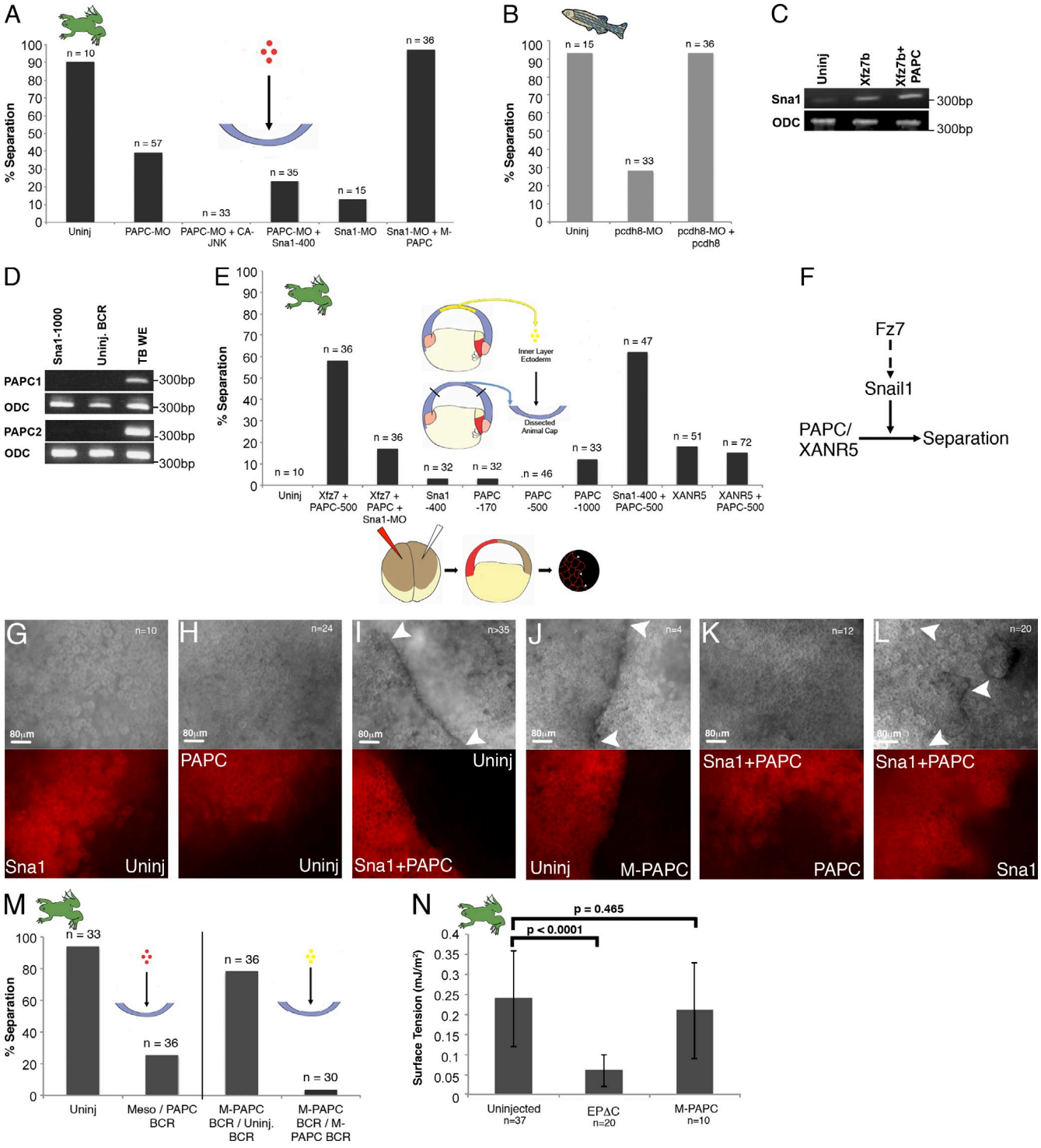

Figure 3. **PAPC in tissue separation.** (A and B) Quantitation of separation behavior; *Xenopus* (A) and zebrafish (B) mesoderm test explants on BCR/epiblast. (C and D) RT-PCR of variously injected *Xenopus* BCR at stage 10 to detect Xsnail1 or PAPC mRNA. TB WE, tailbud stage whole embryo. (E) Ectopic separation behavior in *Xenopus* BCR. Variously injected BCR test explants were placed on uninjected BCR. (F) Inferred control pathway. (G–L) Ectopic cleft formation in *Xenopus* BCR. One side of prospective BCR was injected with RDA, cleft was observed in incident light (arrowheads, top), and cell sorting in red fluorescence (bottom). n, number of explants. (M) Quantitation of separation behavior. (left) *Xenopus* mesoderm on PAPC-injected BCR; (right) M-PAPC BCR on uninjected or M-PAPC BCR. (N) Tissue surface tension of uninjected BCR or BCR expressing DN C-cadherin or M-PAPC. n, number of cell aggregates. Standard deviations are indicated.

completely on occasion (Fig. 4, B, C, and E; Fig. S4 C; and Video 4). Once initiated, cleft contacts expanded rapidly in size during cell attachment, consistent with their adhesive role (Fig. 4 D). Contacts were sensitive to PAPC-MO (Fig. 4, C and E; Fig. S4 C; and Videos 5 and 6). Thus, PAPC function is both necessary and sufficient for cleft contacts to form between cells with different PAPC expression, ascribing to PAPC a role in self/non–self-recognition.

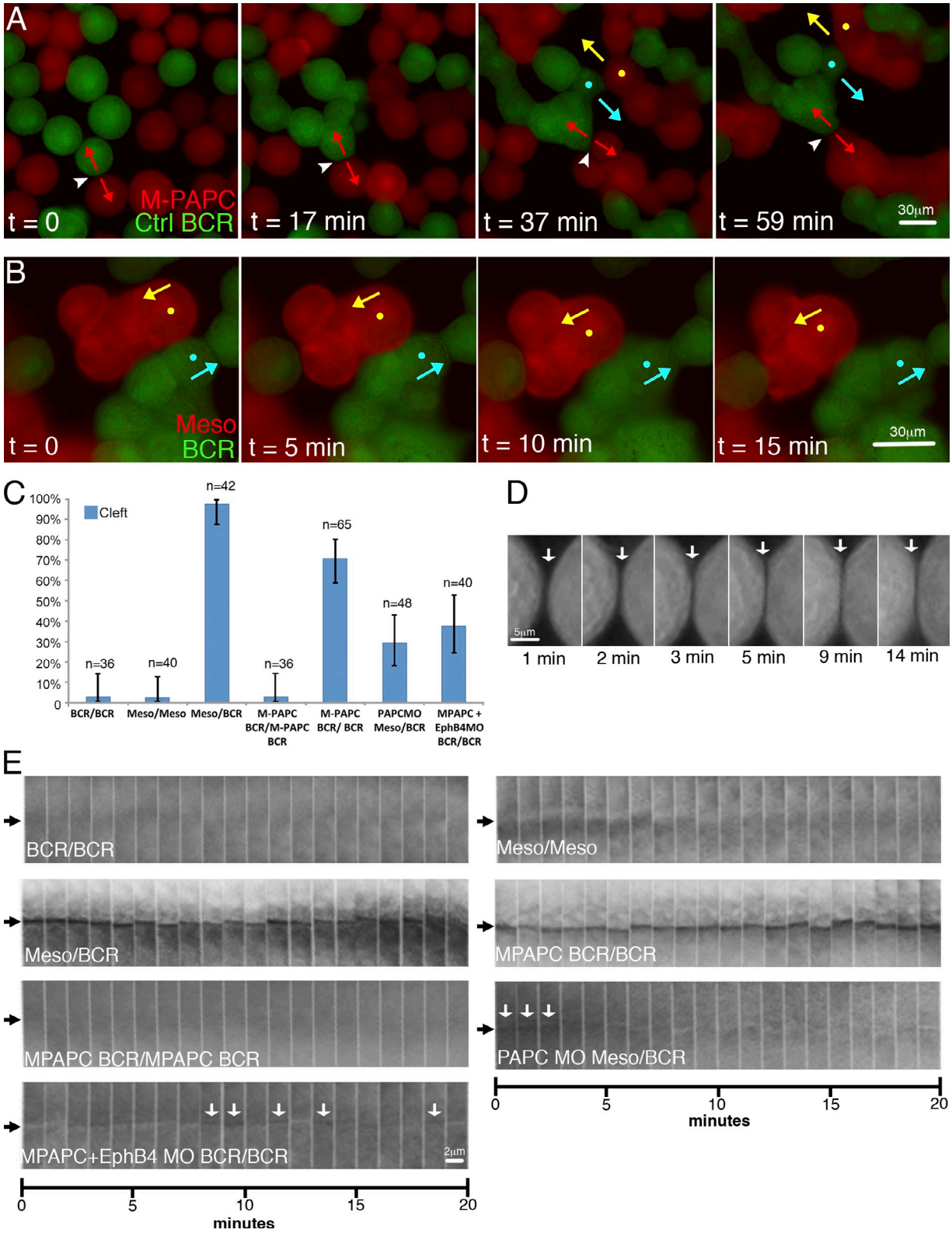

Figure 4. **Cleft contact formation.** (A) Reaggregation of normal (FDA labeled) and M-PAPC–expressing (RDA) BCR cells. Arrowheads indicate example of cleft contact; blue and yellow dots and arrows indicate gliding movement; cell groups move apart in the direction of the red arrows. (B) Reaggregating prechordal mesoderm (RDA) and BCR (FDA) cells. Gliding of cells marked as in A. (C) Frequency of cleft contacts after 30 min of reaggregation. 95% confidence intervals indicated; n, number of cell pairs. (D) Expansion of initial cleft contact (arrows) between reaggregating ectoderm and mesoderm cells. (E) Exemplary kymographs of cell contacts in reaggregated cells quantitated in C. Black arrows indicate the position of cell–cell contact. White or gray, close contact; dark, cleft contact (pointed out by white arrows when only occasionally present).

Inhibition of PCP signaling downstream of PAPC

To analyze downstream effects of PAPC/Snail1 during tissue separation, we explored a seemingly paradoxical finding: Dvl2 was required for Xsnail1 expression, but Dvl2-MO did not block separation behavior (Fig. 5 A). One possibility is that Dvl2-MO inhibited Xsnail1 expression but rescued separation further downstream; indeed, Dvl2-MO rescued separation in Xsnail1-MO–injected as well as PTX-treated mesoderm (Fig. 5 A). The PCP component Prickle (Pk1) is up-regulated in *Xenopus* mesoderm (Takeuchi et al., 2003; Veeman et al., 2003) and in the axial mesoderm of zebrafish (Carreira-Barbosa et al., 2003). Pk1 knockdown, which neither blocked separation (Fig. 5 A) nor reduced Xsnail1 expression (Fig. S5 A), also rescued separation. The PCP component Vangl2/Stbm had similar effects (Fig. 5 A). In the zebrafish, Dvl2-MO and Pk-MO likewise rescued tissue separation (Fig. 5 B and Fig. S1 H).

In *Xenopus* two Xfz7 isoforms exist, Xfz7a and Xfz7b (Wheeler and Hoppler, 1999; Djiane et al., 2000; Medina et al., 2000). Xfz7b is required for Xsnail1 expression, and its knockdown does not rescue the loss of Xsnail1 function. However, knockdown of closely related Xfz7a rescued separation in Xsnail1-MO embryos (Fig. 5 A). Thus, interference with main components of the PCP complex is sufficient to promote separation behavior in the mesoderm.

PAPC/Snail1 did not noticeably affect expression of PCP components (Fig. S5, B and C), suggesting that it inhibited PCP signaling functionally (Fig. 5 C). To characterize PCP inhibition, we reconstituted the mesoderm–BCR boundary in vitro (Fig. 5 D; Rohani et al., 2011). Dvl2-GFP or Pk1-venus localized to membrane puncta in the mesoderm (Fig. 5, E and F). Knockdown of Pk1 reduced Dvl puncta and vice versa (Fig. S5, D and H), indicating a mutual dependence. Strikingly, both Dvl and Pk puncta were diminished in the mesoderm at membranes bordering the BCR (Fig. 5, E and F). In contrast, Dvl2-GFP puncta did form on the BCR side of the boundary (Fig. 5 I and Fig. S5 E).

In the mesoderm, Dvl2-GFP puncta appeared at the boundary, but moved rapidly away from the membrane and vanished (Fig. 5, G and I; and Video 7). PAPC-MO stabilized puncta (Fig. 5, H and I; and Video 8), suggesting that PAPC normally prevents their accumulation at the boundary. Likewise, in Xsnail1 morphants, Pk1 and Dvl2 puncta increased in number in the mesoderm adjacent to the BCR, and cells of the two tissues interdigitated (Fig. 5 I and Fig. S5, F and G). Coinjection of Dvl2-MO with Xsnail1-MO reduced Pk1 puncta across the entire mesoderm (Fig. S5 H), and their absence from the boundary (Fig. 5 I) is consistent with the rescue of separation. Knockdown of XANR5 increased puncta numbers at the boundary, and the effect of Xsnail1-MO on puncta was partially reversed by XANR5 mRNA (Fig. 5 I and Fig. S5, J and K), showing partially redundant XANR5 and Snail1 functions. Puncta were localized on explant surfaces (Fig. 5 I and Fig. S5 L), suggesting that their absence from the boundary is not a consequence of, but rather a prerequisite for cleft formation. M-PAPC expression in the BCR also diminished Dsh puncta at the induced cleft (Fig. 5 I and Fig. S5 M).

PCP signaling has been implicated in cell adhesion (see Discussion). When we knocked down Dvl2 or Pk1 in mesoderm explants or in the embryo, cell separation generated pronounced retraction fibers (Fig. 6, A–F), reminiscent of the membrane tethers between detaching mesoderm and BCR cells at Brachet's cleft (Rohani et al., 2011). In addition, tissue surface tension, a measure of cell adhesion, was diminished in the mesoderm by Pk1-MO (Fig. 6 G), and Pk1-MO–injected cells showed reduced mixing with uninjected cells (Fig. 6 H). In contrast, injection of ephrinB1-MO increased surface tension (Fig. 6 G), consistent with Eph/ephrin signaling normally lowering mesoderm cohesion (Rohani et al., 2014). We propose that PCP puncta strengthen adhesion within the mesoderm to counteract the effects of Eph/ephrin and that their down-regulation at the mesoderm–ectoderm boundary permits tissue separation. Removal of Dvl puncta from the boundary-apposed membranes of cells, but not from interior membranes, is compatible with the simultaneous requirement for Dvl2 in Snail1 expression. Its role as an EphB-interacting protein (Tanaka et al., 2003) in the context of tissue separation remains to be elucidated.

A Snail1-independent function of PAPC is required for tissue separation

PCP inhibition is not sufficient for boundary formation. In gain-of-function experiments, coinjection of Dvl2-MO and PAPC, but not Dvl2-MO alone, induced separation (Fig. 7 A). Moreover, when Dvl2-MO was expressed in half of the BCR, no boundary formed, but a cleft appeared when PAPC was coexpressed; the boundary vanished when PAPC was simultaneously expressed in the other half of the BCR (Fig. 7, B–D). These results confirm that Xsnail1 can be functionally replaced by Dvl2 inhibition. Importantly, they also show that PAPC has a function beyond PCP inhibition. This was also evident in reaggregation experiments. Dvl2-MO–injected BCR cells attached to uninjected cells to form close contacts, and the coexpression of PAPC was required to induce cleft contact formation (Fig. 7, E and F). The function of PAPC in this process does not depend on Snail1.

Eph/ephrin function is likewise required in addition to PCP inhibition. When EphB4 was knocked down in the mesoderm such that tissue separation was inhibited (Rohani et al., 2011), Dvl puncta remained sparse at the boundary (Figs. 6 I and 7 G). This result confirms that reduced puncta density is not a consequence of cleft formation, and it places EphB signaling in parallel to PCP inhibition. Consistent with this notion, injection of Xsnail1 mRNA or of Dvl2-MO did not rescue separation upon EphB4 knockdown, whereas separation behavior induced by Dvl2-MO/PAPC expression in the BCR was inhibited by EphB4-MO (Fig. 7 H). In conclusion, PCP inhibition is required for cleft formation but is not sufficient: PAPC has an essential role in addition to its PCP-inhibitory function, a role in which Eph/ephrin signaling is required. Our overall findings on the regulation of tissue separation at Brachet's cleft are summarized in a model (Fig. 7 I) discussed below.

Structure of cleft contacts

To analyze cell–cell interactions across ectoderm–mesoderm boundaries at high resolution, we performed transmission

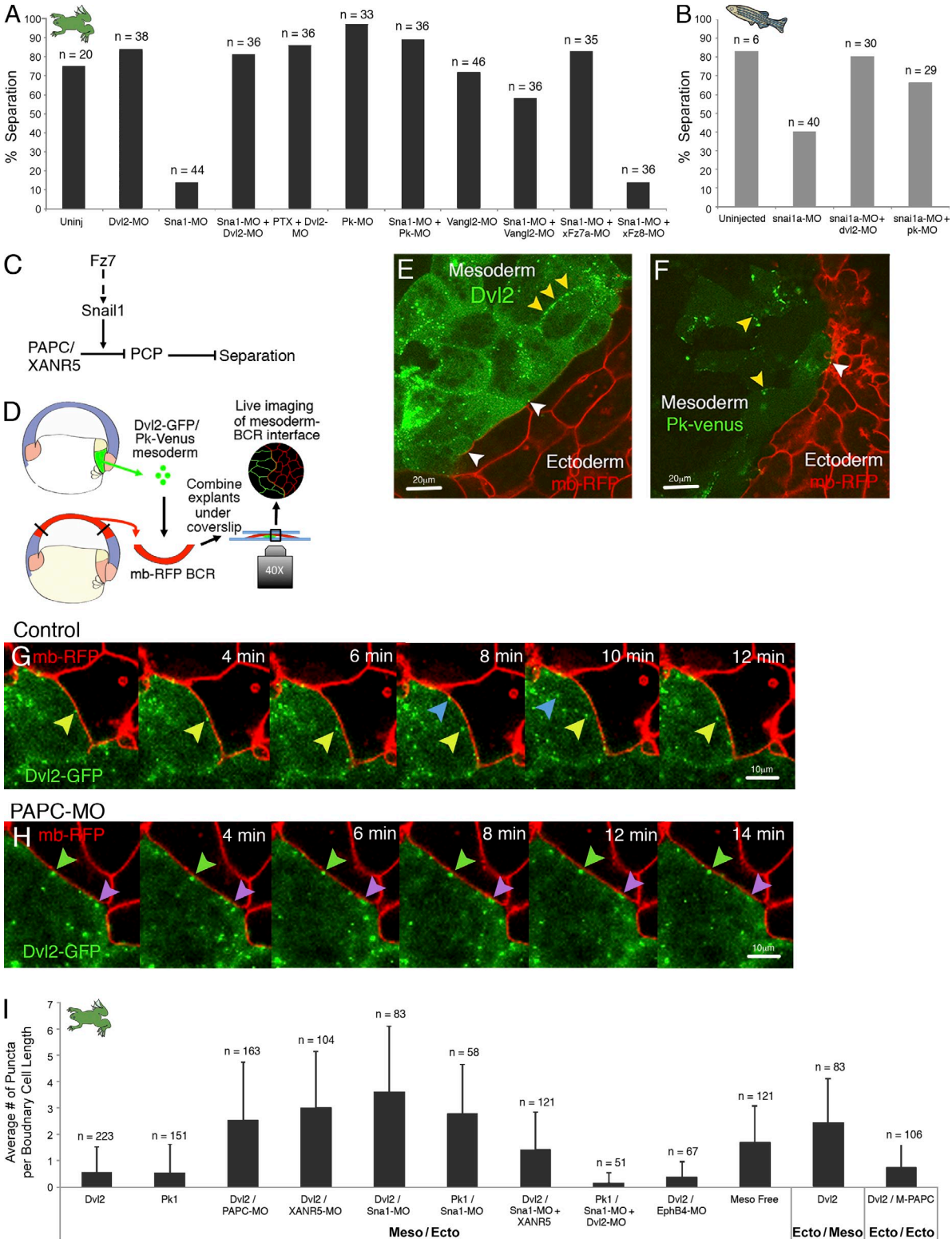

Figure 5. **PAPC-dependent PCP inhibition at boundary.** (A and B) Quantitation of tissue separation using *Xenopus* (A) and zebrafish (B) mesoderm test explants. (C) Inferred control pathway. (D–F) Localization of Dvl2-GFP and Pk1-venus in *Xenopus*. Yellow arrowheads indicate puncta in mesoderm (green); white arrowheads indicate boundary to ectoderm; ectoderm is labeled with membrane-RFP (red). 27 (E) and 20 (F) explant boundaries were evaluated in I. (G and H) Behavior of Dvl-GFP puncta at boundary to ectoderm in normal (G) or PAPC-MO–injected mesoderm (H). Arrowheads: blue, puncta appears, moves to interior, and disappears; yellow, moves to interior and stays; green, stable puncta; purple, cluster of fusing puncta. Of a total of 27 (G) or 18 (H) explant boundaries, 4 and 3, respectively, were filmed. (I) Puncta per cell at boundary. n, number of cells examined at 9–27 different explant boundaries per experimental treatment. Standard deviations indicate variability between individual cells. Averages are increased significantly compared with mesoderm Dvl-GFP or Pk1-venus at boundary (first two columns; *t* test, $P < 0.0001$ in all cases) except M-PAPC in ectoderm (last column, $P = 0.111$).

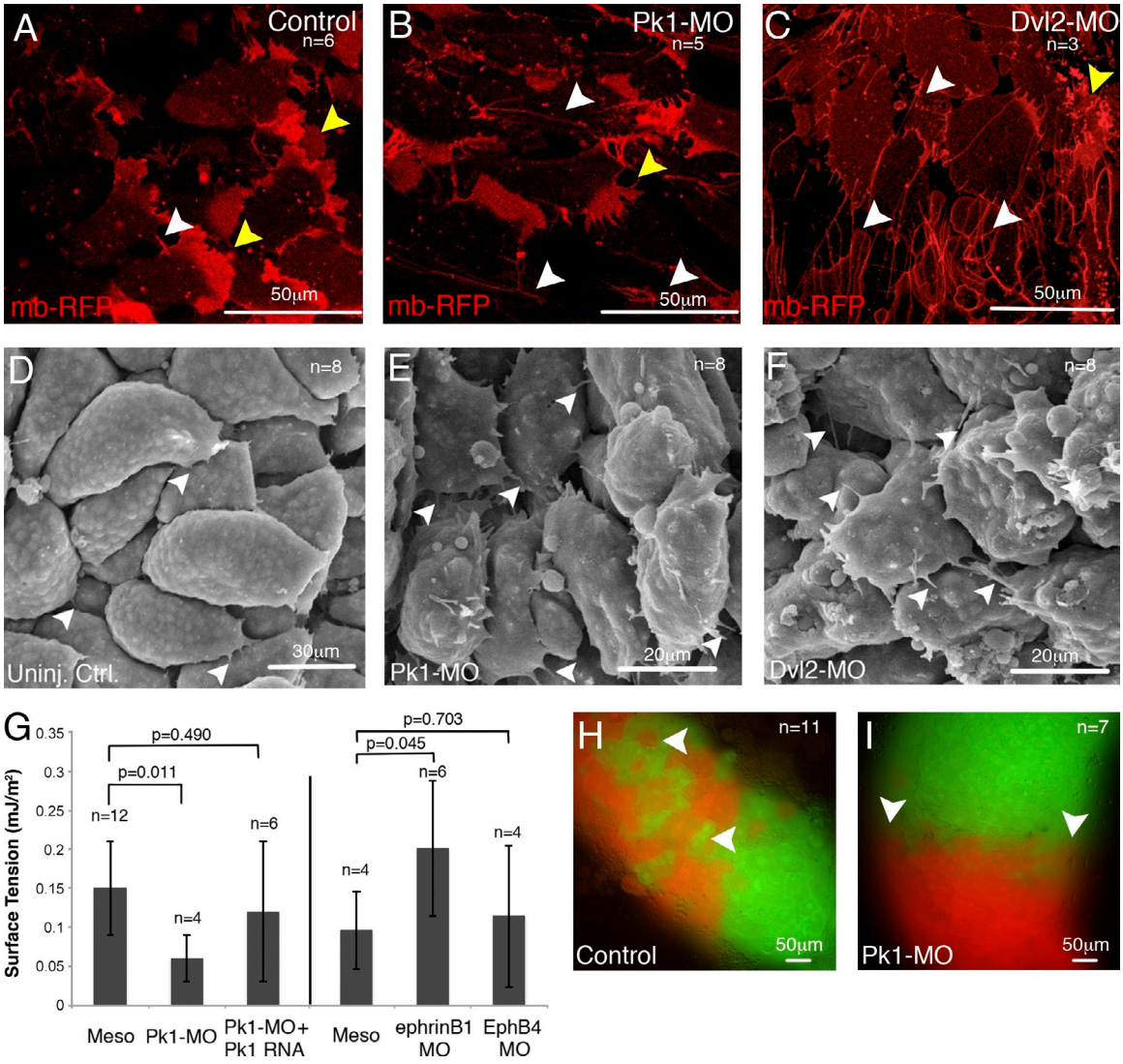

Figure 6. **PCP function strengthens cell adhesion.** (A–C) Prechordal mesoderm explants. Frames from time-lapse recordings of membrane-RFP–labeled cells migrating over each other. White arrowheads indicate membrane tethers in Pk1-MO or Dvl2-MO explants; yellow arrowheads indicate lamellipodia. n, number of explants. (D–F) Prechordal mesoderm in SEM images of sagittally fractured gastrulae. Extensions similar to membrane tethers in A–C are frequent in Pk1-MO or Dvl2-MO embryos (arrowheads). n, number of embryos. (G) Tissue surface tension in prechordal mesoderm is decreased by Pk1-MO and increased by ephrinB1-MO. Standard deviations are indicated. n, number of aggregates from a single experiment. (H) Normal mixing (arrowheads) of left and right prechordal mesoderm cells (RDA and FDA labeled) across midline. (I) Cells respect sorting boundary (arrowheads) when Pk1-MO is injected into the RDA side. n, number of embryos.

EM (TEM). At low magnification, Brachet's cleft appeared as an ECM-filled space of irregular width (Fig. 8 A). Large micrometer-sized gaps were intermixed with narrower contacts (Fig. 8 B), which in turn consisted of intermediate contacts 100–300 nm wide and adherens junction–like close contacts <30 nm wide (Fig. 8, C–E), and compatible with cadherin adhesion (Farquhar and Palade, 1963; Miyaguchi, 2000; Tepass et al., 2000). Close contacts occupied 17 ± 1.5% of the cleft length (n = 12 embryos). At intermediate contacts, membranes of adjacent cells typically ran in parallel, bending sharply when they opened into larger spaces, suggesting that cell adhesion occurred across these contacts.

Between ectoderm–mesoderm cell pairs reaggregated in vitro for 20 min (Fig. 9 A), a similar pattern of contacts was observed. Large gaps were interspersed with intermediate and close adherens junction–like contacts (Fig. 9, B–D). Regularly spaced membranes of intermediate contacts diverged abruptly at the surface of cell pairs or at large gaps (Fig. 9 D), again suggesting an adhesive role for these structures. Patches of ECM decorated free cell surfaces and spanned between membranes up to 0.5 µm apart at contacts (Fig. 9, E and F). Knockdown of PAPC generated long stretches of super-close contacts with separation distances of 10 nm (Fig. 9, G and H). In occasional gaps, dense material resembling compacted ECM was present (Fig. 9 H). In PAPC morphant embryos, the fraction of close contacts at Brachet's cleft increased to 48 ± 4.2% (n = 4 embryos).

Ultrastructural gaps between cell pairs were often narrow and perhaps inconsistent with the pronounced gaps observed by light microscopy. We therefore asked whether exclusion of fluorescent dextran from the cell periphery contributed to how wide gaps appeared. In reaggregated cell pairs, phalloidin staining

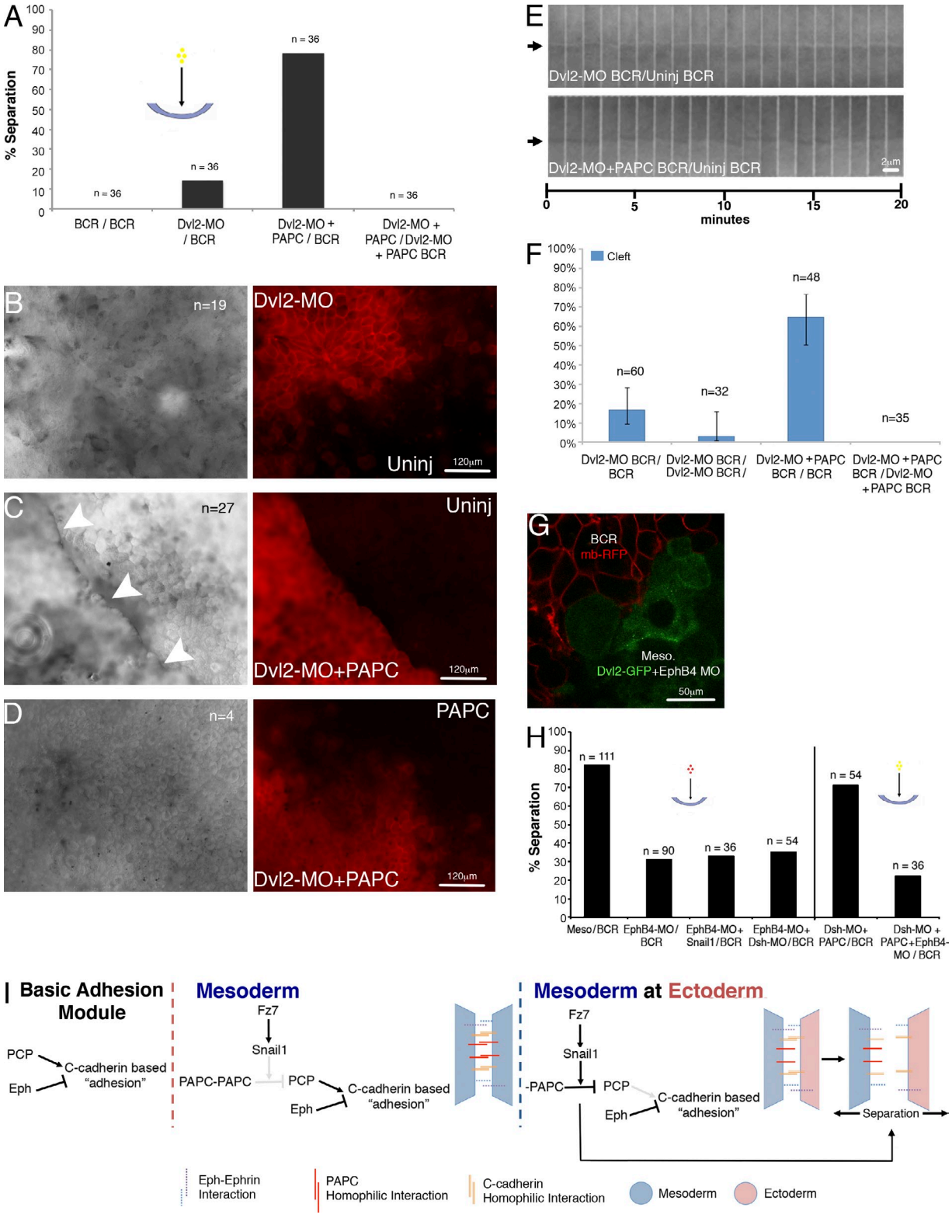

Figure 7. **PAPC function beyond PCP inhibition is required for cleft formation.** (A) Quantitation of separation in gain-of-function experiment. BCR was injected as indicated. (B–D) Ectopic cleft formation in the BCR, as in Fig. 3 (G–L). (E) Exemplary kymographs of cleft contact formation, as in Fig. 4 E. (F) Frequency of cleft contacts after reaggregation, as in Fig. 4 C. (G) Reduced Dvl-GFP puncta in EphB4-MO–injected mesoderm (green) at boundary to BCR (red, membrane-RFP in ectoderm). (H) Quantitation of separation behavior. (left) Mesoderm injected as indicated was tested on normal BCR. (right) BCR explants injected as indicated were tested on normal BCR. (I) Model of tissue separation at the mesoderm–ectoderm (BCR) boundary.

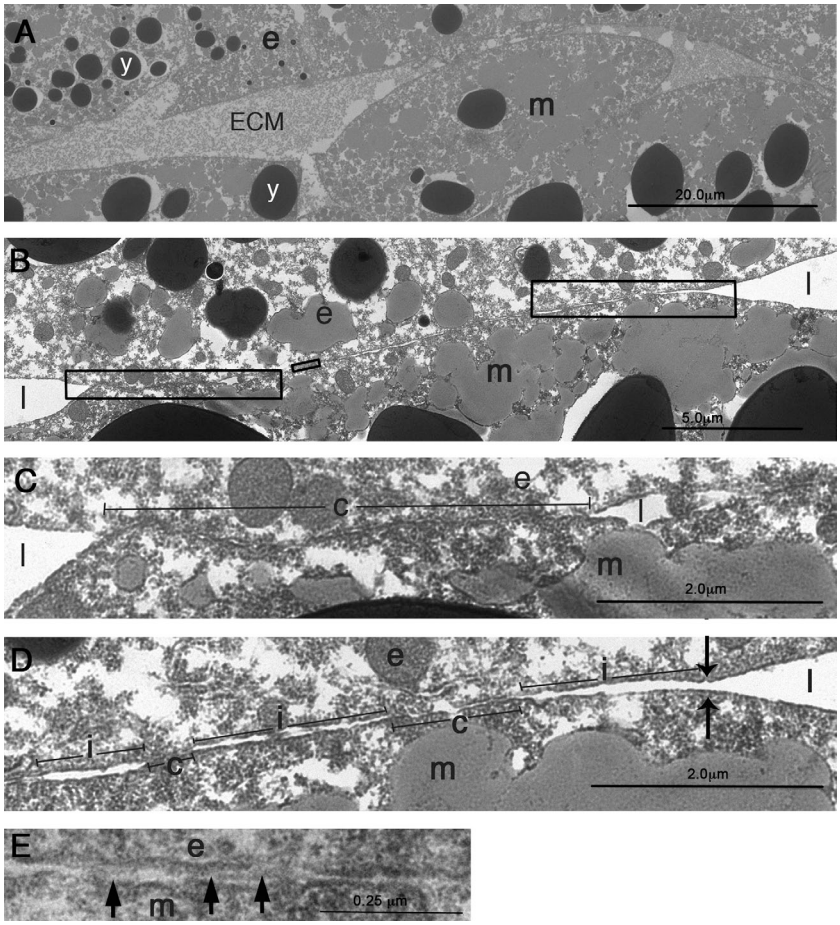

Figure 8. **Ultrastructure of Brachet's cleft.** (A) Low-magnification view of Brachet's cleft. ECM stained with LN. Note size differences of yolk platelets (y) in mesoderm versus ectoderm. (B–E) Contacts between ectoderm and mesoderm cell in absence of ECM staining. Boxes in B indicate regions shown at higher magnification in D–E. e, ectodermal BCR; m, prechordal mesoderm; l, large gaps; i, intermediate, gap-like contacts; c, close, adherens junction–like contacts. Arrows in D indicate point of divergence of membranes at end of intermediate contact and in E indicate characteristics of adherens junctions at high cadherin density.

revealed prominent F-actin cortices (Fig. 10, A–D). Between ectoderm–ectoderm or mesoderm–mesoderm pairs, no gaps were observed using dextran labeling, and F-actin staining at the interface was very weak (Fig. 10, A and B), consistent with a reduction in cortex density upon adhesion in these cells (David et al., 2014). At ectoderm–mesoderm contacts, F-actin staining overlapped considerably, though not completely, with the dextran-contrasted gaps between cells (Fig. 10, C and C′), in agreement with the presence of both large and narrow gaps at the ultrastructural level. F-actin staining was also peripheral to the dextran label at free cell surfaces above contacts (Fig. 10 D). Exclusion of dextran from the cortices of ectoderm–mesoderm pairs was also observed in living cells labeled with LifeAct (Fig. 10 E).

In conclusion, cleft contacts comprise a small fraction of adherens junction–like contacts located between stretches of intermediate-sized gaps, which appear to be adhesive, and large micrometer-scale gaps. All gaps are filled with ECM, and their normal maintenance requires PAPC expression. In contrast to contacts between cells of the same type, strong cell cortices are maintained at cleft contacts, which apparently exclude labeled dextran.

Discussion

We identified two roles for PAPC in tissue separation at Brachet's cleft. First, Fz7-dependent Snail1 expression enables PAPC to down-regulate PCP function in the mesoderm specifically at its boundary to the ectoderm, and we argue that this reduces adhesion across the boundary. Second, PAPC is necessary for the formation of a distinct type of cell–cell attachment: cleft contacts. This role is independent of Snail1 but requires Eph signaling and inhibition of PCP function. We synthesized these findings into a model of tissue separation at the ectoderm–mesoderm boundary (Fig. 7 I).

In *Xenopus* and zebrafish, C- and E-cadherin, respectively, ensure cohesion of gastrula tissue on either side of Brachet's cleft (Kühl and Wedlich, 1996; Montero et al., 2005). In *Xenopus* mesoderm, this basic cell–cell adhesion is modulated. Eph/ephrin signaling lowers tissue cohesion, PCP signaling increases it, and the eventual strength of mesoderm cohesion is the result of these opposite effects. Evidence for adhesion promotion by PCP components was presented previously. In the zebrafish, interaction of Wnt11, Fz7, Dvl, and Flamingo (Fmi) increases cell contact persistence at respective puncta (Witzel et al., 2006), and E-cadherin adhesion is strengthened by Pk1a (Oteiza et al., 2010). In *Xenopus*, the PCP protein Fritz strengthens adhesion (Kim et al., 2010). Although we focused on Dvl2 and Pk1 puncta in our analysis, we cannot exclude that adhesion is also affected by diffuse PCP proteins at the cell membrane (Panousopoulou et al., 2013). Cohesion of *Xenopus* chordamesoderm is also modulated by PAPC (Chen and Gumbiner, 2006; Kraft et al., 2012), but our surface tension measurements indicated no general effect of M-PAPC on cohesion. We propose that cadherin-mediated adhesion, its reduction by Ephs/ephrins, and its

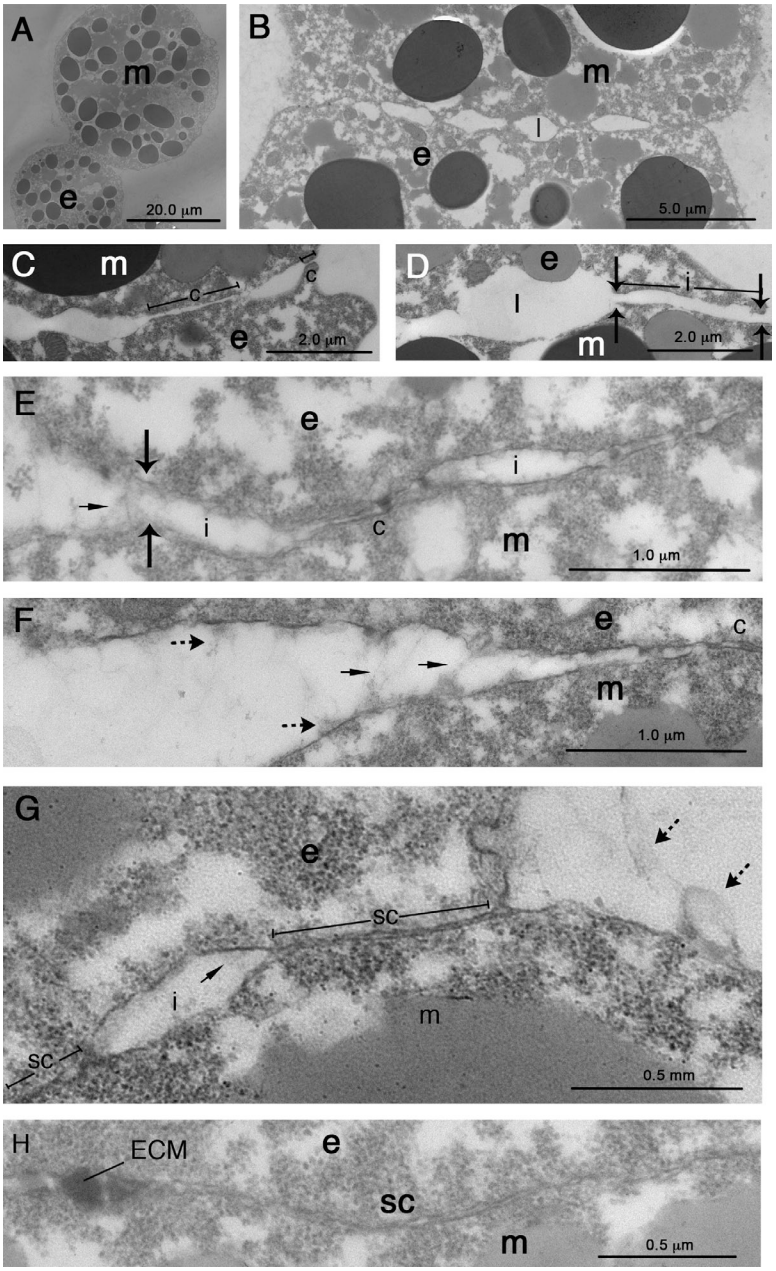

Figure 9. **Ultrastructure of cleft contacts.** Cells after 20 min of reaggregation. (A) Pair of mesoderm (large yolk platelets) and ectoderm cells (small platelets). (B) Alternating large gaps and narrow contacts between cells of ectoderm–mesoderm pair. (C and D) High-magnification views of regions of close (C) and intermediate contacts (D), respectively, of a cell pair. (E and F) Cleft contact ECM stained with lanthanum/alcian blue. ECM stretching across gaps (small arrows) or in patches on cell surface and in large gaps (dashed arrows) is shown. (G and H) Contacts between normal ectoderm and PAPC-MO–injected prechordal mesoderm cells, ECM stained with lanthanum/alcian blue. e, ectodermal BCR; m, prechordal mesoderm; l, large gaps; i, intermediate contacts; c, close, adherens junction–like contacts; sc, super-close contacts; large arrows, points of divergence of membranes at end of intermediate contacts.

compensatory up-regulation by PCP signaling represent a basic cohesion module in the mesoderm, and perhaps in the ectoderm (Fig. 7 I).

Boundary formation at Brachet's cleft is not caused by general adhesion differences between tissues, i.e., by differential adhesion (Winklbauer, 2009). Thus, M-PAPC has no effect on tissue cohesion despite the strong induction of cell sorting (Ninomiya and Winklbauer, 2008) and ectopic boundary formation. Conversely, differential adhesiveness in *Xenopus* gastrulae induced by manipulations of cadherin expression does not promote cell sorting in the intact embryo and generates indistinct sorting boundaries in vitro (Ninomiya et al., 2012). Moreover, Eph/ephrin signaling is strongest and PCP puncta are diminished specifically at the cleft. Together, these findings suggest that tissue separation relies on local cell interactions at the boundary and not on overall cohesion differences.

At the core of boundary cell interaction lays a self/non–self-recognition function of PAPC (Fig. 7 I). We showed that the apposition of $PAPC^+$ and $PAPC^-$ cells is not only essential for normal tissue separation, but also at ectopic boundaries in the ectoderm, and in the chordamesoderm (Ninomiya et al., 2012). Apparently, PAPC does not mediate the interaction between specific cell types, but controls a self/non–self-recognition process that discriminates between $PAPC^+$ and $PAPC^-$ cells, leading to the formation of close contacts between cells of the same type and of cleft contacts between different types.

We propose that a difference between trans-binding and free PAPC is essential for recognition (Fig. 7 I). PAPC–PAPC interaction can occur within the mesoderm, but not at contacts with nonexpressing cells. In a population of Snail1-enabled PAPC cells, non-enabled PAPC in adjacent cells suffices to disrupt their separation. Even the secreted extracellular domain of PAPC prompts cell

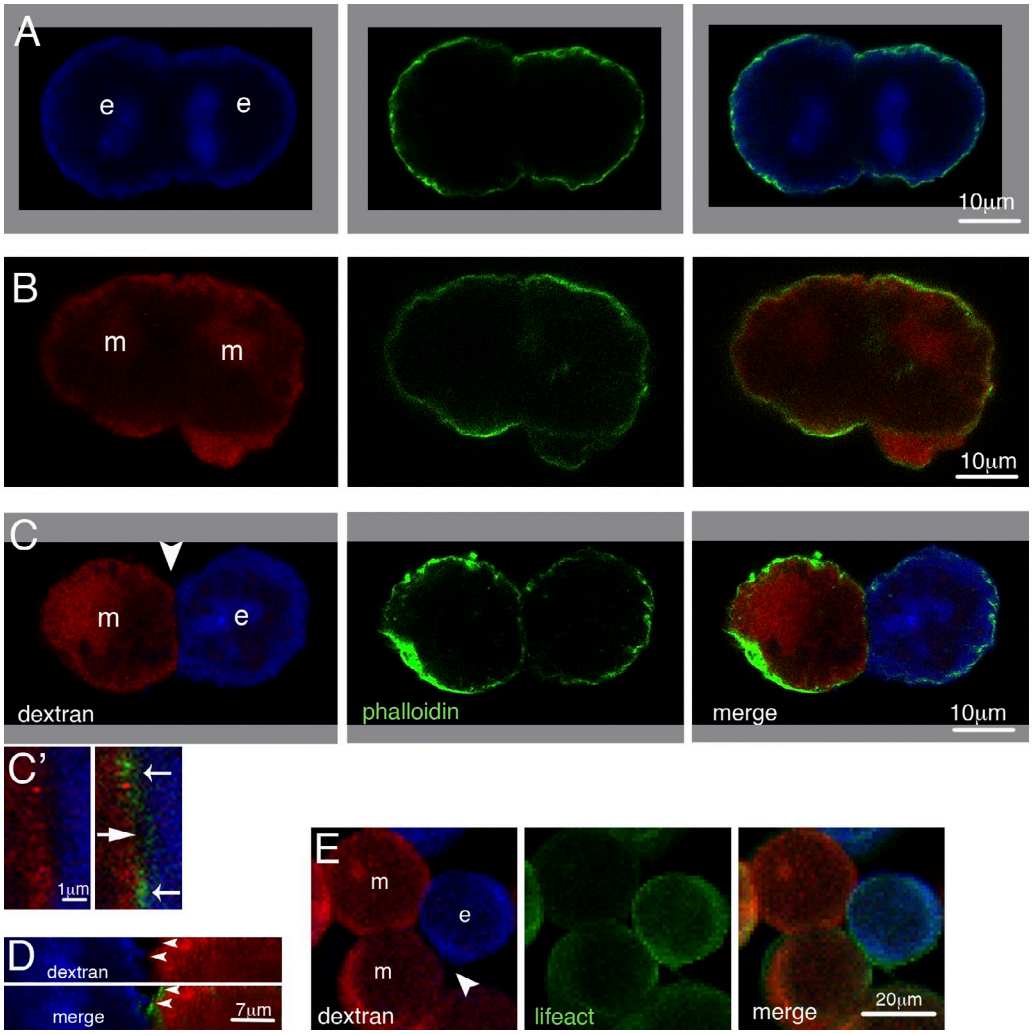

Figure 10. **Actin cortex at cleft contacts.** (A–C) Ectoderm–ectoderm (A), mesoderm–mesoderm (B), and ectoderm–mesoderm (C) reaggregating cells filled with cascade blue–dextran (blue; ectoderm) or RDA (red; mesoderm) and stained with fluorescein-tagged phalloidin for F-actin cortex labeling. Arrowhead in C indicates a cleft contact. (C′) High-magnification view of part of cleft contact in C; small arrows indicate gap largely covered by phalloidin staining; large arrow indicates gap remaining between cortices of adjacent cells. (D) Z stack of cleft contact; F-actin staining (bottom) is peripheral to RDA (top and bottom) boundary (arrowheads) both above cleft (top arrowheads) and in cleft (bottom arrowheads). (E) GFP-LifeAct (green) in gap (arrowhead) between living mesoderm and ectoderm cells labeled as in A–D.

dispersal in an M-PAPC–expressing patch (Kim et al., 1998), suggesting that any occupancy of the PAPC extracellular domain by a homophilic binding partner disrupts its function in separation.

PCP puncta are present on the free surface of explants. Apparently, cells distinguish between neighbors lacking PAPC and the absence of adjacent cells altogether. Because ectopic boundaries can be induced in ectoderm and chordamesoderm, the required interaction between tissues should not be very specific. In *Xenopus*, PAPC interacts indirectly with ubiquitously expressed C-cadherin (Chen et al., 2009), and seeding M-PAPC–expressing BCR cells on a substratum of purified C-cadherin permits M-PAPC to reduce adhesion to this substratum (Chen and Gumbiner, 2006), probably mimicking conditions at the boundary. Thus, cadherin interaction at the boundary may be required to alert $PAPC^+$ cells to the presence of $PAPC^-$ cells (Fig. 7 I).

The PAPC recognition process triggers two independent effects (Fig. 7 I). First, PCP signaling is inhibited and Dvl and Pk1 puncta are reduced on the $PAPC^+$ side of the tissue interface. A possible mechanism could be based on the physical interaction between the extracellular PAPC domain and Fz7 (Medina et al., 2004; Kraft et al., 2012). Binding of Fz7a to free PAPC could remove it from its PCP function. Such an effect could become independent of Snail1 at high PAPC concentrations and be responsible for PAPC-mediated BCR cell sorting (Chen and Gumbiner, 2006). Together with elevated Eph/ephrin signaling, local inhibition of the PCP adhesive function is bound to create a line of weak tissue cohesion. This is not sufficient, however, as no ectopic boundary forms between Dvl-depleted and normal ectoderm. Second, PAPC is needed to establish cleft contacts (Fig. 7 I). This function does not require Snail1 to enable PAPC; addition of PAPC to Dvl-MO cells is sufficient. Moreover, PCP inhibition does not require Eph signaling, whereas cleft contact formation does, confirming that the two effects of PAPC recognition are independent processes.

PAPC-dependent cleft contact formation constitutes a peculiar adhesive interaction where cells attach but can easily slip past each other. Adherens junction–like close contacts should contribute to cell attachment and allow for Eph/ephrin signaling across clefts. These contacts are infrequent, however, and they could permit lateral cell gliding by forming and dissolving rapidly. Pk/Dvl puncta have been implicated in contact persistence in zebrafish (Witzel et al., 2006), and we speculate that they could stabilize cadherin-based close contacts within a tissue, but not at the boundary where puncta are reduced. The increase of close contacts at the boundary upon PAPC knockdown increases puncta frequency, supporting this hypothesis. The simultaneous appearance of large blobs of extracellular material in gaps between cells suggests that PAPC may also regulate ECM distribution on cell surfaces at the cleft.

Actin cortex density is inversely correlated with adhesiveness in *Xenopus* gastrula cells (David et al., 2014). The presence of a stronger and perhaps more contractile cortex between mesoderm and ectoderm cells, as compared with homotypic cell pairs, would also be consistent with less adhesive and more dynamic cell contacts at the mesoderm–ectoderm interface, as indicated by lateral gliding of cells or their spontaneous detachments in mixed ectoderm/mesoderm cell reaggregates.

Clustering of cell adhesion receptors is often driven by anti-adhesive steric hindrance of close contacts in the regions between adhesion domains (Sackmann and Smith, 2014). Interestingly, however, the geometry of intermediate contacts suggests that they mediate adhesion, and lanthanum/alcian blue staining is consistent with an adhesive ECM or glycocalyx. However, we cannot exclude cell–cell attachment by very large nonclassical cadherins (e.g., Kazmierczak et al., 2007). Cell–ECM adhesion is common, but cell–cell adhesion mediated by an intervening thin layer of ECM is not well described other than in sponges, where large extracellular proteoglycan complexes are bound by cell surface receptors (Bucior and Burger, 2004; Bucior et al., 2004). Nonetheless, the combination of facilitated shear movement and substantial adhesion at cleft contacts seems well suited for mesoderm translocation on the BCR during gastrulation, and intermediate contact adhesion may essentially contribute to this property.

The PAPC/Snail1 module, PCP inhibition, and Eph signaling seem to collaborate during tissue separation at other cleft-like boundaries. PAPC and Snail1 are involved in notochord–somite boundary formation in *Xenopus* and zebrafish (unpublished data), and Snail1 expression determines this boundary in *Ciona* (Fujiwara et al., 1998). The requirement for Eph/ephrin signaling in *Xenopus* (Fagotto et al., 2013) and the absence of PCP puncta from this boundary in zebrafish (Yin et al., 2008) and *Ciona* (Jiang et al., 2005) are consistent with this hypothesis. PAPC, Snail1, and Eph/ephrin signaling are also required for somite segmentation (Holley, 2007). However, the specific roles of these components may differ in the different systems. For example, Snail1 expression on both sides of the boundary interferes with notochord–somite separation (Fujiwara et al., 1998), whereas PAPC does not (unpublished data). Examining these differences may lead to a deeper understanding of Snail1 and PAPC function during tissue separation at Brachet's cleft.

Materials and methods

Embryos and injections

Xenopus embryos were obtained and injected as described previously (Luu et al., 2008). *Xenopus* embryos obtained from in vitro fertilized eggs were dejellied with 2% cysteine in 1/10× modified Barth's solution (MBS; 88 mM NaCl, 1 mM KCl, 2.4 mM $NaHCO_3$, 0.82 mM $MgSO_4$, 0.33 mM $Ca(NO_3)_2$, 0.41 mM $CaCl_2$, 10 mM Hepes [+NaOH], 1% streptomycin, and 1% penicillin, pH 7.4) with the pH adjusted to 8. After washing, embryos were cultured in 1/10× MBS in a 15°C incubator and staged according to Nieuwkoop and Faber (1967). Embryos at the 4-cell stage were injected in both dorsal blastomeres or animally into all four blastomeres using a Nanoinject II (Drummond Scientific Company). Embryos were kept in 4% Ficoll during injections. Transgenic CLGY21 (Ellingsen et al., 2005) and AB zebrafish stocks were maintained at 28°C and bred as described previously (Westerfield, 2000). CLGY21 fish carry a retrovirally inserted enhancer detection vector consisting of a murine leukemia virus retroviral vector (pCL) carrying the gene for yellow fluorescent protein and a 1-kb proximal promoter of the zebrafish *GATA2* gene. The transgene is inserted 14,041 bp downstream of the *snail1a* gene on chromosome 11 (Ellingsen et al., 2005). Embryos were obtained from natural spawnings and staged as described previously (Kimmel et al., 1995). Embryos were maintained in embryo medium in a 28.5°C incubator. Microinjections were performed at room temperature, using an MPP1-2 pressure injector (ASI), into the yolk at the 1-cell stage, and embryos were then returned to the 28.5°C incubator (Bruce et al., 2003). Before microsurgery, embryos were manually removed from the chorion in embryos medium using forceps.

Microsurgery and the BCR assay

Microsurgery and the BCR assay in *Xenopus* and zebrafish were performed in MBS at room temperature. Vitellin membranes were removed manually with forceps. In *Xenopus*, the BCR assay was performed as described previously (Wacker et al., 2000): prechordal mesoderm or inner BCR test explants were placed on explanted BCR (typically five test explants per BCR), and after 1 h, test explants were scored for having remained on the surface of the BCR, using Stemi SV11 (Carl Zeiss) or MZ16F (Leica) stereomicroscopes. Each assay was repeated at least six times. The number of explants tested (*n*) is indicated in the respective figures. Statistical significance of differences was confirmed using the paired Student's *t* test (Rohani et al., 2011). For zebrafish, the interior surface of deyolked shield stage CLGY21 embryos served as the ectodermal (epiblast) substratum, and control ectoderm test aggregates were acquired by scraping cells off the inner surface. For mesoderm aggregates, 70% epiboly stage CLGY21 embryos were bisected with a tungsten wire and deyolked, and dorsal anterior mesoderm cells were scraped off. Aggregates were placed onto prepared ectodermal caps, coverslipped, and scored as in *Xenopus*, using an Imager Z1 compound microscope (Carl Zeiss) with a 20× Plan-Apochromat objective, numerical aperture 0.75, and an Orca-ER camera (Hamamatsu Photonics) using Volocity 6.0 (PerkinElmer) software.

Reaggregation

Excised tissues from fluorescein-dextran (FDA)–, cascade blue–dextran-, or rhodamine-dextran (RDA)–injected embryos were dissociated in Ca^{2+}-free MBS, and cells were mixed and filmed (two to three independent repetitions per treatment) while reaggregating in MBS in BSA-coated dishes at room temperature using an Axiovert 200M inverted microscope with a 20× Plan-Neofluar objective, numerical aperture 0.5, an AxioCam MRm, and AxioVision 4.8 image processing software (all Carl Zeiss).

Tissue surface tension

Tissue surface tension was measured using axisymmetric drop shape analysis (ADSA; del Río and Neumann, 1997; Luu et al., 2011). At equilibrium, the drop shape of a tissue explant reflects a compromise between tissue surface tension and gravity and is described by the Laplace equation of capillarity. The ADSA program numerically integrates the Laplace equation to generate theoretical drop shapes for different hypothetical surface tensions and optimizes the surface tension to find the shape that best fits an experimental drop profile. To obtain explant profiles, we combined small excised pieces of tissue collected from one (ectoderm) or three (mesoderm) embryos in a plasticine well for 1 h to form an aggregate, placed the aggregates (10–37 ectoderm and 4–12 mesoderm aggregates per treatment) on nonadhesive poly-2-hydroxyethyl methacrylate substrate for 2 h at room temperature, fixed them in 4% formaldehyde in MBS, and imaged the drop-shaped aggregates from the side in a 45° mirror using a Stemi SV11 stereomicroscope and AxioCam MRc camera (both Carl Zeiss). We determined the

density of explants from different regions according to Ninomiya and Winklbauer (2008). Explants were placed in MBS layered on top of a mixture of MBS and Ficoll (19%, 20%, 21%, 22%, or 23%) in 1.5-ml centrifugation tubes and centrifuged at 100 *g* for 3 min. Explants were either sinking to the bottom or floating at the interface depending on the Ficoll mixture, whose density was determined by weighing a defined volume. We fitted explant profiles and explant densities using ADSA to obtain surface tension values.

Constructs, morpholinos, and inhibitors

For morpholinos, constructs, and concentrations used, refer to Tables S1–S4. The Xsnail1-MO overlaps the ATG start codon. It fully recognizes the mRNAs of both closely related (98% identity) *Xenopus* Snail1 genes (X53450.1, BC056857.1 and NM_001086456.1), but not the in vitro synthesized Xsnail1 mRNA used for injection. Chelerythrine was used at 6 µM and SP600125 at 10 µM.

In situ hybridization

In situ hybridization on *Xenopus* embryos was modified after Harland (1991). gsc pBluescript SK(−) (H. Steinbeisser, Heidelberg University, Heidelberg, Germany) was linearized with EcoR1 and Xbra DB30 pSP73 (M. Sargent, Medical Research Council National Institute for Medical Research, Mill Hill, London, England, UK) with Bgl2 (GE Healthcare), and digoxigenin-labeled antisense probe was synthesized using T7 RNA polymerase (mMessage mMachine; Ambion). Sna probe was generated using Bgl2 (GE Healthcare)-digested pMX51 and SP6 RNA polymerase (mMessage mMachine). Embryos were fixed in MEMFA for 1–2 h at room temperature, dehydrated in ethanol, and stored at −20°C. They were rehydrated in PBS/Tween, incubated with Proteinase K, rinsed with triethanolamine, refixed with 4% formaldehyde, prehybridized for 4 h at 60°C in 50% formamide, 5× SSC, 1 mg/ml Torula RNA, 100 µg/ml heparin, 1× Denhart's, 0.1% Tween-20, 0.1% CHAPS, and 10 mM EDTA, and incubated with probe overnight at 60°C in hybridization buffer (prehybridization buffer plus 0.5 mg/ml tRNA). After washes in 2× SSC solutions and maleic acid buffer, probe was detected by incubating embryos with a 1:2,000 dilution of anti-digoxigenin AP, fab fragments of antibody from sheep (Roche) for 4 h, and washing with maleic acid buffer overnight and briefly with alkaline phosphatase buffer. Embryos were incubated in BM purple (Roche), and the color reaction was monitored and stopped with MEMFA. Between 18 and 58 specimens from at least two batches of embryos were examined for each treatment, 127 from uninjected controls, and photographed using a Stemi SV11 stereomicroscope and AxioCam MRc camera. Whole-mount in situ hybridization on zebrafish embryos was performed as described previously (Jowett and Lettice, 1994). Antisense probe was synthesized from EcoRI-digested pBS-*snail1a* (G. Kelly, Western University, London, Ontario, Canada) transcribed with T3 RNA polymerase. Embryos were fixed overnight at 4°C in 4% PFA, rinsed in PBT, and stored overnight at −20°C in 100% methanol. After rehydration into PBT, embryos were post-fixed for 20 min at room temperature in 4% PFA followed by PBT washes. Embryos were prehybridized for 3 h at 70°C in 65% formamide, 5× SSC, 50 µg/ml heparin, 0.1% Tween-20, and 9 mM citric acid, incubated with probe overnight at 70°C in hybridization buffer (prehybridization buffer plus 0.5 mg/ml tRNA), and washed in 2× SSC solutions and PBT. Probe was detected by incubating embryos overnight at 4°C with a 1:5,000 dilution of anti–digoxigenin-AP, fab fragments of antibody from sheep (Roche). After PBT washes, embryos were incubated with NBT/BCIP (Roche), and the color reaction was monitored and stopped by PBT washes. Between 35 and 67 embryos from at least two batches were examined for each treatment and 191 uninjected controls. Embryos in 80% glycerol were photographed at 5× on an MZ16F stereomicroscope with a Plan-Apochromat 1.0× objective using a MicroPublisher 3.3 camera (QImaging) using Openlab.

RT-PCR

RT-PCR was performed at least twice for each experiment. For primers and temperatures used, see Table S3.

Scanning EM (SEM)

Xenopus and zebrafish embryos were processed for SEM as in Damm and Winklbauer (2011). Embryos were fixed in 2.5% glutaraldehyde (GA) in 0.1 M sodium cacodylate buffer (CB) overnight at 4°C, post-fixed in osmium tetroxide (Structure Probe) for 1 h at 4°C, washed in distilled water for 30 min, and dehydrated in an ethanol dehydration series (50% ethanol in 0.1 M cacodylate for 20 min, 100% ethanol twice for 20 min) and in hexamethyldisilazane (a 1:1 dilution of hexamethyldisilazane and ethanol for 30 min followed by 100% hexamethyldisilazane twice for 30 min). The specimens were left to dry overnight, mounted on SEM stubs using conductive carbon tape (Structure Probe), and sputter coated with gold-palladium (60%/40%) for 50 s. Specimens were imaged with a Hitachi S-2500 scanning electron microscope.

TEM

Stage 11 *Xenopus* embryos were fixed overnight at 4°C in 3% GA and 2% PFA in 0.05 M CB, pH 7.0, either with (seven embryos) or without (seven uninjected and four PAPC-MO–injected embryos) 1% lanthanum nitrate (LN) as an ECM stain (Johnson, 1977). Embryos were then rinsed in 0.1 M CB, pH 7.0, cut in half along the sagittal plane, and fixed overnight at 4°C in 0.1 M CB containing 1% OsO_4 or 1% OsO_4 and 1% LN if previously treated with LN. After rinsing with 0.1 M CB, embryos were dehydrated in a graded series of ethanol, embedded in 100% Spurr's resin, and cured at 65°C for 24 h. Ultrathin (90–100 nm) sections were obtained using an EM UC6 microtome (Leica) and stained with 3% uranyl acetate in methanol for 1 h and Reynold's lead citrate for 10 min. About 10–15 ectoderm–prechordal mesoderm cell contacts were present per embryo.

Cell reaggregate sample preparation was modified from a yeast cell protocol by Wright et al. (1988). BCR and mesoderm from stage 11 *Xenopus* embryos were dissociated and reaggregated as described in the "Reaggregation" section. Cells were allowed to reaggregate for 20 min on a glass-bottom Petri dish coated with 1% BSA. Cell reaggregates were then fixed in 0.05 M CB containing 3% GA and 2% PFA, either with or without 1% alcian blue as an enhancer for LN ECM staining, for 30 min at room temperature (Shea, 1971). Cells were rinsed with 0.1 M CB and embedded in 3% low-melt agarose overnight at room temperature. Slices containing embedded cells were excised, placed bottom-up in a Petri dish, and covered with a thin layer of 3% low-melt agarose with a glass coverslip on top. After 4 h at 4°C, slices containing embedded cells were excised and fixed for 1 h at room temperature in 1% OsO_4 in 0.1 M CB or 1% OsO_4 and 1% LN in 0.1 M CB if previously treated with alcian blue. Samples were then washed with 0.1 M CB, dehydrated in a graded ethanol series, and embedded in 100% Spurr's resin. Ultrathin (90–100 nm) sections were obtained using an EM UC6 microtome. Two re-embedded agarose blocks were sectioned for each treatment (normal cells with and without LN/alcian blue staining and cells from PAPC-MO–injected embryos). Ultrathin sections were stained with 3% uranyl acetate in methanol for 1 h and Reynold's lead citrate for 10 min. TEM images were collected on a Hitachi HT7700 microscope at 80.0 kV. 15 LN/alcian blue–stained ectoderm–prechordal mesoderm cell pairs, 6 unstained pairs, and 10 pairs with PAPC-MO–injected prechordal mesoderm were inspected closely. Ectoderm and mesoderm cells were distinguished by the size of yolk platelets (Nakatsuji, 1975) and ectodermal pigment granules.

Fluorescence microscopy

To visualize Pk1 or Dvl2 puncta, embryos were injected with Pk1-venus, Dvl2-GFP, or membrane-RFP with or without Xsnail1-, Pk1-, or Dvl-MOs. Mesoderm pieces were explanted at stage 10, covered with ectodermal BCR, and gently pressed down with a piece of coverslip. Images were taken at room temperature from an Axiovert 100M LSM 510 confocal microscope (Carl Zeiss) at 40× magnification (Plan-Neofluar 40×/1.3 oil objective) using a PMT and LSM 3.2 WNT4.0 software (Carl Zeiss) to process images. The F-actin cortex in reaggregating cells was visualized by FITC-phalloidin staining of fixed cells (four experiments) or by expression of LifeAct in living cells (four experiments). For image collection, a TCS SP8 confocal microscope (Leica) with 20×/0.75 oil immersion, 63×/1.4 oil immersion, and 100×/1.4 oil immersion objectives and LasAF 3.2.0.9652 software or an Axiovert 100M LSM 510 confocal microscope at 40× magnification (Plan-Neofluar 40×/1.3 oil objective) using a PMT and LSM 3.2 WNT4.0 software was used. To visualize ectopic boundaries in the BCR, the border between uninjected and injected sides was visualized under incident light illumination, and in parallel by fluorescence microscopy to detect injected RDA, using an Axiovert 200M microscope with 20× Plan-Neofluar/0.5 objective, AxioCam MDm camera, and AxioVision 4.8 image processing software (all Carl Zeiss). To visualize the cell membranes of migrating prechordal mesoderm cells, embryos were injected with mRNA encoding membrane-RFP, and explants of the mesoderm were combined with BCR explants to induce directional cell migration (Damm and Winklbauer, 2011). Cells were observed using an Axiovert 100M LSM 510 laser-scanning confocal microscope at 40× magnification (Plan-Neofluar 40×/1.3 oil objective), using a PMT and LSM 3.2 WNT4.0 software to process images.

Online supplemental material

Fig. S1 shows that mesoderm marker gene expression is not affected by Xsnail1 knockdown and that snai1a mediates tissue separation in the zebrafish gastrula. Fig. S2 shows that PAPC and Snail1 control tissue

separation without modulating Eph/ephrin expression. Fig. S3 demonstrates that complementary ectopic Snail1 and PAPC expression can generate a sorting boundary but not a cleft-like boundary. Fig. S4 provides details on cell sorting and gap contact formation between PAPC-expressing and -nonexpressing cells. Fig. S5 shows additional data on PCP inhibition at the tissue boundary. Tables S1 and S2 list the morpholinos and constructs used in this study, respectively. Table S3 lists the RT-PCR primers and annealing temperatures used in this study. Table S4 lists the constructs used for *Xenopus* and zebrafish experiments. Video 1 shows reaggregating BCR cells injected with M-PAPC mRNA and RDA (red) or FDA (green). Video 2 shows the same sequence in grayscale mode. Video 3 shows reaggregating cells similar to Video 1, except that M-PAPC–expressing cells were coinjected with EphB4-MO. Video 4 presents reaggregating prechordal mesoderm cells (RDA injected, red) and ectodermal BCR cells (FDA, green). Video 5 shows reaggregating mesoderm and BCR cells as in Video 4, but with PAPC-MO having been injected into mesoderm cells. Video 6 shows the same sequence as Video 5 but in the grayscale mode. Video 7 shows the behavior of Dvl2-GFP puncta (green) in mesoderm cells at the boundary to the ectodermal BCR where cell membranes are labeled with membrane-RFP (red). Video 8 shows the behavior of Dvl2-GFP puncta as in Video 7, but with PAPC-MO being injected into mesoderm cells. Online supplemental material is available at http://www.jcb.org/cgi/content/full/jcb.201409026/DC1.

We thank F. Fagotto, R. Habas, G. Kelly, R. Moon, M. Sargent, H. Steinbeisser, and E. Nishida for reagents and Henry Hong and Audrey Darabie of the CSB Imaging Facility for help with TEM and confocal microscopy.

This work was supported by grant MOP-53075 from the Canadian Institutes of Health Research to R. Winklbauer, grant 458019 from the Natural Sciences and Engineering Research Council of Canada to A.E.E. Bruce, and grant 019355 from the Canadian Cancer Society to R. Winklbauer and A.E.E. Bruce.

The authors declare no competing financial interests.

Submitted: 4 September 2014
Accepted: 12 February 2015

References

Barrallo-Gimeno, A., and M.A. Nieto. 2005. The Snail genes as inducers of cell movement and survival: implications in development and cancer. *Development*. 132:3151–3161. http://dx.doi.org/10.1242/dev.01907

Bikkavilli, R.K., M.E. Feigin, and C.C. Malbon. 2008. $G\alpha_o$ mediates WNT–JNK signaling through dishevelled 1 and 3, RhoA family members, and MEKK 1 and 4 in mammalian cells. *J. Cell Sci.* 121:234–245. http://dx.doi.org/10.1242/jcs.021964

Boutros, M., N. Paricio, D.I. Strutt, and M. Mlodzik. 1998. Dishevelled activates JNK and discriminates between JNK pathways in planar polarity and wingless signaling. *Cell*. 94:109–118. http://dx.doi.org/10.1016/S0092-8674(00)81226-X

Bruce, A.E., C. Howley, Y. Zhou, S.L. Vickers, L.M. Silver, M.L. King, and R.K. Ho. 2003. The maternally expressed zebrafish T-box gene eomesodermin regulates organizer formation. *Development*. 130:5503–5517. http://dx.doi.org/10.1242/dev.00763

Bucior, I., and M.M. Burger. 2004. Carbohydrate–carbohydrate interactions in cell recognition. *Curr. Opin. Struct. Biol.* 14:631–637. http://dx.doi.org/10.1016/j.sbi.2004.08.006

Bucior, I., S. Scheuring, A. Engel, and M.M. Burger. 2004. Carbohydrate–carbohydrate interaction provides adhesion force and specificity for cellular recognition. *J. Cell Biol.* 165:529–537. http://dx.doi.org/10.1083/jcb.200309005

Carreira-Barbosa, F., M.L. Concha, M. Takeuchi, N. Ueno, S.W. Wilson, and M. Tada. 2003. Prickle 1 regulates cell movements during gastrulation and neuronal migration in zebrafish. *Development*. 130:4037–4046. http://dx.doi.org/10.1242/dev.00567

Chen, X., and B.M. Gumbiner. 2006. Paraxial protocadherin mediates cell sorting and tissue morphogenesis by regulating C-cadherin adhesion activity. *J. Cell Biol.* 174:301–313. http://dx.doi.org/10.1083/jcb.200602062

Chen, X., E. Koh, M. Yoder, and B.M. Gumbiner. 2009. A protocadherin-cadherin-FLRT3 complex controls cell adhesion and morphogenesis. *PLoS ONE*. 4:e8411. http://dx.doi.org/10.1371/journal.pone.0008411

Chung, H.A., T.S. Yamamoto, and N. Ueno. 2007. ANR5, an FGF target gene product, regulates gastrulation in *Xenopus*. *Curr. Biol.* 17:932–939. http://dx.doi.org/10.1016/j.cub.2007.04.034

Damm, E.W., and R. Winklbauer. 2011. PDGF-A controls mesoderm cell orientation and radial intercalation during *Xenopus* gastrulation. *Development*. 138:565–575. http://dx.doi.org/10.1242/dev.056903

David, R., O. Luu, E.W. Damm, J.W.H. Wen, M. Nagel, and R. Winklbauer. 2014. Tissue cohesion and the mechanics of cell rearrangement. *Development*. 141:3672–3682. http://dx.doi.org/10.1242/dev.104315

del Río, O.I., and A.W. Neumann. 1997. Axisymmetric Drop Shape Analysis: computational methods for the measurement of interfacial properties from the shape and dimensions of pendant and sessile drops. *J. Colloid Interface Sci.* 196:136–147. http://dx.doi.org/10.1006/jcis.1997.5214

Djiane, A., J. Riou, M. Umbhauer, J. Boucaut, and D. Shi. 2000. Role of frizzled 7 in the regulation of convergent extension movements during gastrulation in *Xenopus laevis*. *Development*. 127:3091–3100.

Ellingsen, S., M.A. Laplante, M. König, H. Kikuta, T. Furmanek, E.A. Hoivik, and T.S. Becker. 2005. Large-scale enhancer detection in the zebrafish genome. *Development*. 132:3799–3811. http://dx.doi.org/10.1242/dev.01951

Essex, L.J., R. Mayor, and M.G. Sargent. 1993. Expression of *Xenopus* snail in mesoderm and prospective neural fold ectoderm. *Dev. Dyn.* 198:108–122. http://dx.doi.org/10.1002/aja.1001980205

Fagotto, F., N. Rohani, A.-S. Touret, and R. Li. 2013. A molecular base for cell sorting at embryonic boundaries: contact inhibition of cadherin adhesion by ephrin/Eph-dependent contractility. *Dev. Cell*. 27:72–87. http://dx.doi.org/10.1016/j.devcel.2013.09.004

Farquhar, M.G., and G.E. Palade. 1963. Junctional complexes in various epithelia. *J. Cell Biol.* 17:375–412. http://dx.doi.org/10.1083/jcb.17.2.375

Fujiwara, S., J.C. Corbo, and M. Levine. 1998. The snail repressor establishes a muscle/notochord boundary in the Ciona embryo. *Development*. 125:2511–2520.

Habas, R., Y. Kato, and X. He. 2001. Wnt/Frizzled activation of Rho regulates vertebrate gastrulation and requires a novel Formin homology protein Daam1. *Cell*. 107:843–854. http://dx.doi.org/10.1016/S0092-8674(01)00614-6

Hammerschmidt, M., and C. Nüsslein-Volhard. 1993. The expression of a zebrafish gene homologous to *Drosophila* snail suggests a conserved function in invertebrate and vertebrate gastrulation. *Development*. 119:1107–1118.

Harland, R.M. 1991. In situ hybridization: an improved whole-mount method for *Xenopus* embryos. *Methods Cell Biol.* 36:685–695. http://dx.doi.org/10.1016/S0091-679X(08)60307-6

Holley, S.A. 2007. The genetics and embryology of zebrafish metamerism. *Dev. Dyn.* 236:1422–1449. http://dx.doi.org/10.1002/dvdy.21162

Hukriede, N.A., T.E. Tsang, R. Habas, P.L. Khoo, K. Steiner, D.L. Weeks, P.P. Tam, and I.B. Dawid. 2003. Conserved requirement of Lim1 function for cell movements during gastrulation. *Dev. Cell*. 4:83–94. http://dx.doi.org/10.1016/S1534-5807(02)00398-2

Jiang, D., E.M. Munro, and W.C. Smith. 2005. Ascidian prickle regulates both mediolateral and anterior-posterior cell polarity of notochord cells. *Curr. Biol.* 15:79–85. http://dx.doi.org/10.1016/j.cub.2004.12.041

Johnson, K.E. 1977. Extracellular matrix synthesis in blastula and gastrula stages of normal and hybrid frog embryos. I. Toluidine blue and lanthanum staining. *J. Cell Sci.* 25:313–322.

Jowett, T., and L. Lettice. 1994. Whole-mount in situ hybridizations on zebrafish embryos using a mixture of digoxigenin- and fluorescein-labelled probes. *Trends Genet.* 10:73–74. http://dx.doi.org/10.1016/0168-9525(94)90220-8

Kazmierczak, P., H. Sakaguchi, J. Tokita, E.M. Wilson-Kubalek, R.A. Milligan, U. Müller, and B. Kachar. 2007. Cadherin 23 and protocadherin 15 interact to form tip-link filaments in sensory hair cells. *Nature*. 449:87–91. http://dx.doi.org/10.1038/nature06091

Kim, G.-H., and J.-K. Han. 2005. JNK and ROKα function in the noncanonical Wnt/RhoA signaling pathway to regulate *Xenopus* convergent extension movements. *Dev. Dyn.* 232:958–968. http://dx.doi.org/10.1002/dvdy.20262

Kim, S.-H., A. Yamamoto, T. Bouwmeester, E. Agius, and E.M. Robertis. 1998. The role of paraxial protocadherin in selective adhesion and cell movements of the mesoderm during *Xenopus* gastrulation. *Development*. 125:4681–4690.

Kim, S.K., A. Shindo, T.J. Park, E.C. Oh, S. Ghosh, R.S. Gray, R.A. Lewis, C.A. Johnson, T. Attie-Bittach, N. Katsanis, and J.B. Wallingford. 2010. Planar cell polarity acts through septins to control collective cell movement and ciliogenesis. *Science*. 329:1337–1340. http://dx.doi.org/10.1126/science.1191184

Kim, S.Y., S. Yasuda, H. Tanaka, K. Yamagata, and H. Kim. 2011. Non-clustered protocadherin. *Cell Adhes. Migr.* 5:97–105. http://dx.doi.org/10.4161/cam.5.2.14374

Kimmel, C.B., W.W. Ballard, S.R. Kimmel, B. Ullmann, and T.F. Schilling. 1995. Stages of embryonic development of the zebrafish. *Dev. Dyn.* 203:253–310. http://dx.doi.org/10.1002/aja.1002030302

Knöchel, S., A. Schuler-Metz, and W. Knöchel. 2000. c-Jun (AP-1) activates BMP-4 transcription in *Xenopus* embryos. *Mech. Dev.* 98:29–36. http://dx.doi.org/10.1016/S0925-4773(00)00448-2

Kraft, B., C.D. Berger, V. Wallkamm, H. Steinbeisser, and D. Wedlich. 2012. Wnt-11 and Fz7 reduce cell adhesion in convergent extension by sequestration of PAPC and C-cadherin. *J. Cell Biol.* 198:695–709. http://dx.doi.org/10.1083/jcb.201110076

Kühl, M., and D. Wedlich. 1996. *Xenopus* cadherins: sorting out types and functions in embryogenesis. *Dev. Dyn.* 207:121–134. http://dx.doi.org/10.1002/(SICI)1097-0177(199610)207:2<121::AID-AJA1>3.0.CO;2-J

Liu, W., A. Sato, D. Khadka, R. Bharti, H. Diaz, L.W. Runnels, and R. Habas. 2008. Mechanism of activation of the Formin protein Daam1. *Proc. Natl. Acad. Sci. USA*. 105:210–215. http://dx.doi.org/10.1073/pnas.0707277105

Luu, O., M. Nagel, S. Wacker, P. Lemaire, and R. Winklbauer. 2008. Control of gastrula cell motility by the Goosecoid/Mix.1/ Siamois network: basic patterns and paradoxical effects. *Dev. Dyn.* 237:1307–1320. http://dx.doi.org/10.1002/dvdy.21522

Luu, O., R. David, H. Ninomiya, and R. Winklbauer. 2011. Large-scale mechanical properties of *Xenopus* embryonic epithelium. *Proc. Natl. Acad. Sci. USA*. 108:4000–4005. http://dx.doi.org/10.1073/pnas.1010331108

Manning, M.L., R.A. Foty, M.S. Steinberg, and E.M. Schoetz. 2010. Coaction of intercellular adhesion and cortical tension specifies tissue surface tension. *Proc. Natl. Acad. Sci. USA*. 107:12517–12522. http://dx.doi.org/10.1073/pnas.1003743107

Medina, A., W. Reintsch, and H. Steinbeisser. 2000. *Xenopu*s frizzled 7 can act in canonical and non-canonical Wnt signaling pathways: implications on early patterning and morphogenesis. *Mech. Dev.* 92:227–237. http://dx.doi.org/10.1016/S0925-4773(00)00240-9

Medina, A., R.K. Swain, K.-M. Kuerner, and H. Steinbeisser. 2004. *Xenopus* paraxial protocadherin has signaling functions and is involved in tissue separation. *EMBO J.* 23:3249–3258. http://dx.doi.org/10.1038/sj.emboj.7600329

Miyaguchi, K. 2000. Ultrastructure of the zonula adherens revealed by rapid-freeze deep-etching. *J. Struct. Biol.* 132:169–178. http://dx.doi.org/10.1006/jsbi.2000.4244

Mlodzik, M. 2002. Planar cell polarization: do the same mechanisms regulate *Drosophila* tissue polarity and vertebrate gastrulation? *Trends Genet.* 18:564–571. http://dx.doi.org/10.1016/S0168-9525(02)02770-1

Montero, J.A., L. Carvalho, M. Wilsch-Bräuninger, B. Kilian, C. Mustafa, and C.P. Heisenberg. 2005. Shield formation at the onset of zebrafish gastrulation. *Development*. 132:1187–1198. http://dx.doi.org/10.1242/dev.01667

Nakatsuji, N. 1975. Studies on the gastrulation of amphibian embryos: Cell movement during gastrulation in *Xenopus laevis* embryos. *Roux's Arch. Dev. Biol.* 178:1–14.

Nieuwkoop, P.D., and J. Faber, editors. 1967. Normal Table of *Xenopus laevis* (Daudin): A Systematical and Chronological Survey of the Development from the Fertilized Egg Till the End of Metamorphosis. Second edition. North-Holland, Amsterdam. 260 pp.

Ninomiya, H., and R. Winklbauer. 2008. Epithelial coating controls mesenchymal shape change through tissue-positioning effects and reduction of surface-minimizing tension. *Nat. Cell Biol.* 10:61–69. http://dx.doi.org/10.1038/ncb1669

Ninomiya, H., R. David, E.W. Damm, F. Fagotto, C.M. Niessen, and R. Winklbauer. 2012. Cadherin-dependent differential cell adhesion in *Xenopus* causes cell sorting in vitro but not in the embryo. *J. Cell Sci.* 125:1877–1883. http://dx.doi.org/10.1242/jcs.095315

Oteiza, P., M. Köppen, M. Krieg, E. Pulgar, C. Farias, C. Melo, S. Preibisch, D. Müller, M. Tada, S. Hartel, et al. 2010. Planar cell polarity signalling regulates cell adhesion properties in progenitors of the zebrafish laterality organ. *Development*. 137:3459–3468. http://dx.doi.org/10.1242/dev.049981

Panousopoulou, E., R.A. Tyson, T. Bretschneider, and J.B. Green. 2013. The distribution of Dishevelled in convergently extending mesoderm. *Dev. Biol.* 382:496–503. http://dx.doi.org/10.1016/j.ydbio.2013.07.012

Park, E.C., G.S. Cho, G.H. Kim, S.C. Choi, and J.K. Han. 2011. The involvement of Eph-Ephrin signaling in tissue separation and convergence during *Xenopus* gastrulation movements. *Dev. Biol.* 350:441–450. http://dx.doi.org/10.1016/j.ydbio.2010.12.012

Rohani, N., L. Canty, O. Luu, F. Fagotto, and R. Winklbauer. 2011. EphrinB/EphB signaling controls embryonic germ layer separation by contact-induced cell detachment. *PLoS Biol.* 9:e1000597. http://dx.doi.org/10.1371/journal.pbio.1000597

Rohani, N., A. Parmeggiani, R. Winklbauer, and F. Fagotto. 2014. Variable combinations of specific ephrin ligand/Eph receptor pairs control embryonic tissue separation. *PLoS Biol.* 12:e1001955. http://dx.doi.org/10.1371/journal.pbio.1001955

Roszko, I., A. Sawada, and L. Solnica-Krezel. 2009. Regulation of convergence and extension movements during vertebrate gastrulation by the Wnt/PCP pathway. *Semin. Cell Dev. Biol.* 20:986–997. http://dx.doi.org/10.1016/j.semcdb.2009.09.004

Rothbächer, U., M.N. Laurent, M.A. Deardorff, P.S. Klein, K.W. Cho, and S.E. Fraser. 2000. Dishevelled phosphorylation, subcellular localization and multimerization regulate its role in early embryogenesis. *EMBO J.* 19:1010–1022. http://dx.doi.org/10.1093/emboj/19.5.1010

Sackmann, E., and A.-S. Smith. 2014. Physics of cell adhesion: some lessons from cell-mimetic systems. *Soft Matter*. 10:1644–1659. http://dx.doi.org/10.1039/c3sm51910d

Sargent, M.G., and M.F. Bennett. 1990. Identification in *Xenopus* of a structural homologue of the *Drosophila* gene snail. *Development*. 109:967–973.

Schambony, A., and D. Wedlich. 2007. Wnt-5A/Ror2 regulate expression of XPAPC through an alternative noncanonical signaling pathway. *Dev. Cell*. 12:779–792. http://dx.doi.org/10.1016/j.devcel.2007.02.016

Shea, S.M. 1971. Lanthanum staining of the surface coat of cells. Its enhancement by the use of fixatives containing Alcian blue or cetylpyridinium chloride. *J. Cell Biol.* 51:611–620. http://dx.doi.org/10.1083/jcb.51.3.611

Speirs, C.K., K.K. Jernigan, S.-H. Kim, Y.I. Cha, F. Lin, D.S. Sepich, R.N. DuBois, E. Lee, and L. Solnica-Krezel. 2010. Prostaglandin Gβγ signaling stimulates gastrulation movements by limiting cell adhesion through Snai1a stabilization. *Development*. 137:1327–1337. http://dx.doi.org/10.1242/dev.045971

Takeuchi, M., J. Nakabayashi, T. Sakaguchi, T.S. Yamamoto, H. Takahashi, H. Takeda, and N. Ueno. 2003. The prickle-related gene in vertebrates is essential for gastrulation cell movements. *Curr. Biol.* 13:674–679. http://dx.doi.org/10.1016/S0960-9822(03)00245-8

Tanaka, M., T. Kamo, S. Ota, and H. Sugimura. 2003. Association of Dishevelled with Eph tyrosine kinase receptor and ephrin mediates cell repulsion. *EMBO J.* 22:847–858. http://dx.doi.org/10.1093/emboj/cdg088

Tanegashima, K., H. Zhao, and I.B. Dawid. 2008. WGEF activates Rho in the Wnt-PCP pathway and controls convergent extension in *Xenopus* gastrulation. *EMBO J.* 27:606–617. http://dx.doi.org/10.1038/emboj.2008.9

Tepass, U., K. Truong, D. Godt, M. Ikura, and M. Peifer. 2000. Cadherins in embryonic and neural morphogenesis. *Nat. Rev. Mol. Cell Biol.* 1:91–100. http://dx.doi.org/10.1038/35040042

Tepass, U., D. Godt, and R. Winklbauer. 2002. Cell sorting in animal development: signalling and adhesive mechanisms in the formation of tissue boundaries. *Curr. Opin. Genet. Dev.* 12:572–582. http://dx.doi.org/10.1016/S0959-437X(02)00342-8

Thiery, J.P. 2002. Epithelial-mesenchymal transitions in tumour progression. *Nat. Rev. Cancer*. 2:442–454. http://dx.doi.org/10.1038/nrc822

Veeman, M.T., D.C. Slusarski, A. Kaykas, S.H. Louie, and R.T. Moon. 2003. Zebrafish prickle, a modulator of noncanonical Wnt/Fz signaling, regulates gastrulation movements. *Curr. Biol.* 13:680–685. http://dx.doi.org/10.1016/S0960-9822(03)00240-9

Wacker, S., K. Grimm, T. Joos, and R. Winklbauer. 2000. Development and control of tissue separation at gastrulation in *Xenopus*. *Dev. Biol.* 224:428–439. http://dx.doi.org/10.1006/dbio.2000.9794

Wallingford, J.B., S.E. Fraser, and R.M. Harland. 2002. Convergent extension: the molecular control of polarized cell movement during embryonic development. *Dev. Cell*. 2:695–706. http://dx.doi.org/10.1016/S1534-5807(02)00197-1

Westerfield, M. 2000. The Zebrafish Book. A guide for the laboratory use of zebrafish (*Danio rerio*). Fourth edition. University of Oregon Press, Eugene, OR. 323 pp.

Wheeler, G.N., and S. Hoppler. 1999. Two novel *Xenopus* frizzled genes expressed in developing heart and brain. *Mech. Dev.* 86:203–207. http://dx.doi.org/10.1016/S0925-4773(99)00117-3

Winklbauer, R. 2009. Cell adhesion in amphibian gastrulation. *Int. Rev. Cell Mol. Biol.* 278:215–275. http://dx.doi.org/10.1016/S1937-6448(09)78005-0

Winklbauer, R., and R.E. Keller. 1996. Fibronectin, mesoderm migration, and gastrulation in *Xenopus*. *Dev. Biol.* 177:413–426. http://dx.doi.org/10.1006/dbio.1996.0174

Winklbauer, R., A. Medina, R.K. Swain, and H. Steinbeisser. 2001. Frizzled-7 signalling controls tissue separation during *Xenopus* gastrulation. *Nature*. 413:856–860. http://dx.doi.org/10.1038/35101621

Witzel, S., V. Zimyanin, F. Carreira-Barbosa, M. Tada, and C.-P. Heisenberg. 2006. Wnt11 controls cell contact persistence by local accumulation of Frizzled 7 at the plasma membrane. *J. Cell Biol.* 175:791–802. http://dx.doi.org/10.1083/jcb.200606017

Wright, R., M. Basson, L. D'Ari, and J. Rine. 1988. Increased amounts of HMG-CoA reductase induce "karmellae": a proliferation of stacked membrane pairs surrounding the yeast nucleus. *J. Cell Biol.* 107:101–114. http://dx.doi.org/10.1083/jcb.107.1.101

Yin, C., M. Kiskowski, P.A. Pouille, E. Farge, and L. Solnica-Krezel. 2008. Cooperation of polarized cell intercalations drives convergence and extension of presomitic mesoderm during zebrafish gastrulation. *J. Cell Biol.* 180:221–232. http://dx.doi.org/10.1083/jcb.200704150